



AARHUS UNIVERSITY



Coversheet

This is the publisher's PDF (Version of Record) of the article.

This is the final published version of the article.

How to cite this publication:

Haruhide Miyagi and Lars Bojer Madsen (2017). Time-dependent restricted-active-space self-consistent-field theory with space partition, *Physical Review A*, Volume 95, Issue 2, February 2017,

<https://doi.org/10.1103/PhysRevA.95.023415>

Publication metadata

Title:	Time-dependent restricted-active-space self-consistent-field theory with space partition
Author(s):	Haruhide Miyagi and Lars Bojer Madsen
Journal:	<i>Physical Review A</i>
DOI/Link:	https://doi.org/10.1103/PhysRevA.95.023415
Document version:	<i>Publisher's PDF (Version of Record)</i>

©2017 American Physical Society

General Rights

Copyright and moral rights for the publications made accessible in the public portal are retained by the authors and/or other copyright owners and it is a condition of accessing publications that users recognize and abide by the legal requirements associated with these rights.

- Users may download and print one copy of any publication from the public portal for the purpose of private study or research.
- You may not further distribute the material or use it for any profit-making activity or commercial gain
- You may freely distribute the URL identifying the publication in the public portal

If you believe that this document breaches copyright please contact us providing details, and we will remove access to the work immediately and investigate your claim.

If the document is published under a Creative Commons license, this applies instead of the general rights.

Time-dependent restricted-active-space self-consistent-field theory with space partition

Haruhide Miyagi and Lars Bojer Madsen

Department of Physics and Astronomy, Aarhus University, 8000 Aarhus C, Denmark

(Received 28 November 2016; published 21 February 2017)

Aiming at efficient numerical analysis of time-dependent (TD) many-electron dynamics of atoms involving multielectron continua, the TD restricted-active-space self-consistent-field theory with space partition (TD-RASSCF-SP) is presented. The TD-RASSCF-SP wave function is expanded in terms of TD configuration-interaction coefficients with Slater determinants composed of two kinds of TD orbitals: \hat{M} orbitals are defined to be nonvanishing in the inner region (\hat{V}), a small volume around the atomic nucleus, and \check{M} orbitals are nonvanishing in the large outer region (\check{V}). For detailed discussion of the SP strategy, the equations of motion are derived by two different formalisms for comparison. To ensure continuous differentiability of the wave function across the two regions, one of the formalisms makes use of the property of the finite-element discrete-variable-representation (FEDVR) functions and introduces additional time-independent orbitals. The other formalism is more general and is based on the Bloch operator as in the R -matrix theory, but turns out to be less practical for numerical applications. Hence, using the FEDVR-based formalism, the numerical performance is tested by computing double-ionization dynamics of atomic beryllium in intense light fields. To achieve high accuracy, \hat{M} should be set large to take into account the strong many-electron correlation around the nucleus. On the other hand, \check{M} can be set much smaller than \hat{M} for capturing the weaker correlation between the two outgoing photoelectrons. As a result, compared with more accurate multiconfigurational TD Hartree-Fock (MCTDHF) method, the TD-RASSCF-SP method may achieve comparable accuracy in the description of the double-ionization dynamics. There are, however, difficulties related to the stiffness of the equations of motion of the TD-RASSCF-SP method, which makes the required time step for this method smaller than the one needed for the MCTDHF approach.

DOI: [10.1103/PhysRevA.95.023415](https://doi.org/10.1103/PhysRevA.95.023415)

I. INTRODUCTION

Accurate description of multielectron continua remains tremendously challenging in theoretical and numerical investigations of atom-light processes. Several kinds of sequential and nonsequential double-ionization dynamics of an atom followed by single- or multiphoton absorption have been studied for a few decades to unveil the role of the electron correlation in the processes by experiments mainly focusing on the angular and energy distributions of the two photoelectrons. The recent advent of new light sources and technologies [1–5], however, enables more detailed experiments by means of intense attosecond extreme ultraviolet (XUV) pulses to time resolve the electron-ejection processes [6,7]. For the analysis and interpretation of the dynamics to support such modern experiments, it is desirable to develop new time-dependent (TD) theoretical methodologies and models beyond the current standard, i.e., beyond the single-active-electron approximation [8], to deal with multielectron continua accurately.

On the other hand, investigation of elementary processes involving single-electron continua has a long tradition, establishing several useful concepts, models, and numerical methods. The space-partition (SP) concept has been among the most widely used strategies in describing atom-electron collisions since its introduction in the R -matrix theory (see the original papers [9–11] and recent reviews [12,13]), in which the configuration space is usually divided into two parts. A relatively small volume around the nucleus is called the inner region wherein a configuration-interaction (CI) expansion of the many-electron wave function is computationally doable, and thereby the complex electron correlation can be taken fully into account. In the rest of the space, the outer region, only one electron is supposed to exist, and this one collides with and scatters off the atom, and feels a long-range effective

potential without electron-exchange correlation. Although the wave function is defined in such a piecewise manner, the R -matrix matching on the surface dividing the space into the two regions ensures that the wave function is continuously differentiable across the surface.

While the R -matrix theory has been very successful for time-independent (TI) scattering problems for several decades, its potential applicability to TD problems has only recently attracted attention. The TD R -matrix (TDRM) theory was formulated based on the Crank-Nicholson scheme for computing the time evolution of many-electron atoms (see the formulation in Refs. [14,15], and also see its applications in Refs. [16–24]). Soon after, the R -matrix theory including time dependence (RMT) [25–28] was proposed based on the same SP concept with the Bloch operator [29] formalism but directly treating the wave function without the R matrix. The Arnoldi Lanczos scheme [30,31] is exploited in RMT to execute the time propagation more efficiently than in TDRM, and has successfully led to various applications [32–38]. The TD restricted- and generalized-active-space configuration-interaction [TD-(RAS/GAS)CI] approach [39–41] follows the same SP strategy, and is similar to RMT but based on the finite-element discrete-variable-representation (FEDVR) functions (see, e.g., Ref. [42]). The TD analytical R -matrix (ARM) approach [43–47] uses the SP strategy aiming at obtaining (semi)analytical formulas by describing the electron in the outer region in the eikonal-Volkov approximation. Note that the central approximation underlying TDRM, RMT, TD-(RAS/GAS)CI, and ARM, and underpinning their computational and theoretical tractability is the reduction of the many-electron problem to a single-electron problem in the outer region. In other words, it is very difficult to deal with two- or many-electron dynamics in the outer region. Aiming at the description of secondary photoelectrons freed by intense

lasers, continuous efforts have been deployed to extend RMT [48,49].

Another promising wave-function-based methodology to elucidate real-time dynamics of atoms and molecules is TD self-consistent-field (SCF) theory. The multiconfigurational TD Hartree-Fock (MCTDHF) method (see, e.g., Refs. [50–53]) is among the most accurate and widely recognized methodologies. To illustrate the numerical property of the method, consider a calculation of laser-induced dynamics of an N_e -electron atom based on the spin-restricted ansatz with $M(\geq N_e/2)$ spatial orbitals. Each orbital is time dependent and composed of thousands of elementary basis functions, e.g., FEDVR functions, defined in a large volume whose radius is at least a few hundred atomic units. The wave function is expanded in terms of the TD CI-expansion coefficients with the Slater determinants comprising the TD orbitals. Based on the investigations so far (see, e.g., Refs. [40,54–57]), it is known that the MCTDHF calculation could achieve good accuracy by setting $M \geq N_e$ even when the system is exposed to intense fields. This relatively small number of orbitals is a great advantage and is owing to the TD orbitals. The strength of the MCTDHF method against the SP-based methods mentioned above is that, by setting the spatial domain of the orbitals large enough, not only single- but also all multielectron continua are, in principle, taken accurately into account. The MCTDHF method, however, has a serious practical problem; due to the full-CI expansion, the number of electronic configurations exponentially increases with respect to N_e . Hence the method is not easily applicable to systems with more than ten electrons for computing nonperturbative dynamics induced by strong lasers. This difficulty motivated us to generalize the MCTDHF method and develop the TD restricted-active-space self-consistent-field (TD-RASSCF) method [58–60]. Because of a large reduction in the number of configurations, the use of the RAS scheme instead of the full-CI expansion extends the numerical applicability to larger systems while retaining a reasonable accuracy. Several new TD-SCF methodologies have recently been proposed along similar strategies to reduce the number of electronic configurations [61–64]. Still, however, updating $M(\geq N_e)$ spatial orbitals composed of many orbital angular momentum states at each time step in the large volume requires a good amount of overhead and stands in the way of further numerical applications. Moreover, no matter how accurately the multielectron continua can be described, the use of the TD orbitals extending over the whole spatial volume makes it unnecessarily complicated to extract even basic information related to observables. Compared to TDRM, RMT, and TD-(RAS/GAS)CI, it is, for example, not straightforward to obtain even single-ionization probabilities after the end of the laser pulse.

In the TD-RASSCF calculations, $M \geq N_e$ may, as mentioned above, ensure an account for the details of strong correlation among many electrons around the nucleus. The correlation between a few outgoing electrons after intense-laser multiple ionization or electron impact ionization may, however, be weak, because, on top of the very small electron density, continuum electrons likely tend to avoid one another [65] (this is not always the case though; see, e.g., Ref. [66]). There is at least no doubt that single-electron continua always predominate multielectron continua and are of most physical

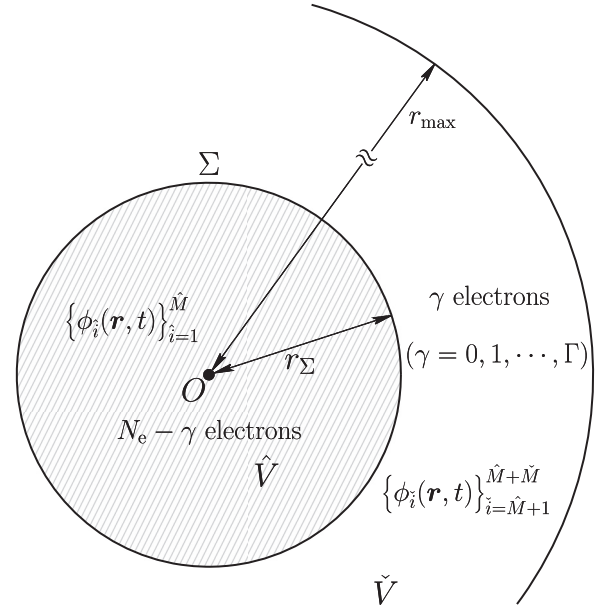


FIG. 1. Basic concept of the TD-RASSCF-SP theory in the description of an N_e -electron atom. The atomic nucleus is set at the origin. The motion of each electron is confined within a large spherical volume of radius $r_{\max} (\gg 1)$, which is, by a small sphere Σ of radius $r_\Sigma (\approx 20\text{--}40)$, divided into two parts: the inner region \hat{V} with radial interval $0 \leq r \leq r_\Sigma$ (shaded volume) and the outer region \check{V} with $r_\Sigma < r \leq r_{\max}$. The TD-RASSCF-SP wave function is expanded in terms of TD CI coefficients with Slater determinants composed of TD orbitals: $N_e - \gamma$ of which are chosen from $\{\phi_i(\mathbf{r}, t)\}_{i=1}^{\hat{M}}$, and γ of which are from $\{\phi_i(\mathbf{r}, t)\}_{i=\hat{M}+1}^{\hat{M}+\check{M}}$, where the two sets of the TD orbitals are nonvanishing only within \hat{V} and \check{V} , respectively. The wave function is a superposition of several different states characterized by γ , where $\gamma = 0, 1, \dots, \Gamma$, with $\Gamma (\leq N_e)$ denoting the maximum number of electrons in \check{V} . Accurate description of double ionization of the atom by moderately strong light fields, for instance, necessitates setting $\Gamma = 2$, and would require the numbers of the TD orbitals to be $\hat{M} \geq N_e$ and $\check{M} \geq \Gamma = 2$.

importance. To describe one- and two-electron ejection in light fields with moderate intensity, the use of as many as $M(\geq N_e)$ orbitals in a large volume may be unnecessary. This estimation naturally motivates us to develop the TD-RASSCF theory with SP (for simplicity henceforth called TD-RASSCF-SP theory), constructing the wave function with many orbitals around the nucleus, but with a small number of orbitals in the vast outer region. Following this basic concept, illustrated in Fig. 1, this paper aims at formulating the TD-RASSCF-SP theory, deriving its working equations, and demonstrating the numerical performance.

This paper is organized as follows. Section II provides several essential definitions for formulating the TD-RASSCF-SP method with FEDVR functions. Section III follows to derive the equations of motion. Section IV then tests the numerical performance for atomic beryllium interacting with strong light fields. The FEDVR-based formalism and its numerical implementations provided in Secs. II, III, and IV prepare for the more general theory presented in Sec. V. In this section, without making use of the property of the FEDVR functions, the TD-RASSCF-SF theory is reformulated

in a more general manner; the Bloch operator in second quantization is the main brick in the construction of the general theory. Section VI concludes this work. Appendix A provides a brief derivation of the equations of motion to complete the Bloch operator-based formalism in Sec. V. Appendix B summarizes the notation rules used throughout this paper. Throughout this paper, atomic units are used unless otherwise specified.

II. PRELIMINARIES

This section provides several definitions that are necessary to formulate the TD-RASSCF-SP theory. Aiming at applications to strong-field and attosecond science, the focus is mainly on describing few-electron-ejection dynamics of an N_e -electron atom in intense laser fields. For simplicity, this paper is devoted to atomic problems based on the spin-

$$\text{Radial interval of } \hat{V}: [0, r_\Sigma] = [r_0, r_1] \cup (r_1, r_2) \cup \dots \cup (r_{\hat{N}_{\text{fe}}-1}, r_{\hat{N}_{\text{fe}}}], \quad (1a)$$

$$\text{Radial interval of } \check{V}: (r_\Sigma, r_{\max}] = (r_{\hat{N}_{\text{fe}}}, r_{\hat{N}_{\text{fe}}+1}) \cup \dots \cup (r_{\hat{N}_{\text{fe}}+\check{N}_{\text{fe}}-1}, r_{\hat{N}_{\text{fe}}+\check{N}_{\text{fe}}}], \quad (1b)$$

where $r_0 = 0$, $r_{\hat{N}_{\text{fe}}} = r_\Sigma$, and $r_{\hat{N}_{\text{fe}}+\check{N}_{\text{fe}}} = r_{\max}$. Defining Lobatto DVR functions with N_{dvr} quadrature points, a set of the FEDVR functions, $\{\chi_k(r)|k=1, \dots, (N_{\text{dvr}}-1)(\hat{N}_{\text{fe}}+\check{N}_{\text{fe}})-1\}$, is composed following the standard prescription (see, e.g., Ref. [42]). In the construction, two Lobatto DVR functions having quadrature points at r_0 and r_{\max} are removed; consequently, every FEDVR function is zero at both edges of the radial interval, i.e., $\chi_k(0) = \chi_k(r_{\max}) = 0$.

The FEDVR functions are then classified into three groups: $\{\chi_k(r)|\hat{k}=1, \dots, (N_{\text{dvr}}-1)\hat{N}_{\text{fe}}-1\}$, $\{\chi_b(r)[\equiv \chi_{(N_{\text{dvr}}-1)\hat{N}_{\text{fe}}}(r)]\}$, and $\{\chi_{\check{k}}(r)|\check{k}=(N_{\text{dvr}}-1)\hat{N}_{\text{fe}}+1, \dots, (N_{\text{dvr}}-1)(\hat{N}_{\text{fe}}+\check{N}_{\text{fe}})-1\}$. Note that the FEDVR functions belonging to the first and third group, respectively, are nonvanishing only below and above r_Σ . On the other hand, the second group only consists of $\chi_b(r)$, which is the bridge function across r_Σ (see, e.g., Ref. [42] for a discussion of the bridge function). For convenience in the formulation below, let \bar{V} be a volume defined such that

$$\text{Radial interval of } \bar{V}: [r_{\hat{N}_{\text{fe}}-1}, r_{\hat{N}_{\text{fe}}}) \cup [r_{\hat{N}_{\text{fe}}}, r_{\hat{N}_{\text{fe}}+1}), \quad (1c)$$

where $\chi_b(r)$ is nonvanishing. Figure 2 illustrates the setup of the FEDVR functions and shows the radial intervals of \hat{V} , \check{V} , and \bar{V} (\bar{V} is not shown in Fig. 1). Each FEDVR function is defined over the whole interval, $[0, r_{\max}]$, albeit nonvanishing only within each particular FE.

B. FEDVR-based orbitals and single-particle Hilbert spaces

As key ingredients in the construction of the wave function based on the spin-restricted ansatz, we define two sets of TD spatial orbitals nonvanishing within \hat{V} and \check{V} , respectively, by

$$\phi_{\hat{i}}(\mathbf{r}, t) = \sum_{\hat{k}\ell m} c_{\hat{k}\ell m}^{\hat{i}}(t) \chi_{\hat{k}}(r) Y_{\ell m}(\Omega) \quad [\hat{i} = 1, \dots, \hat{M} (\geq N_e/2)], \quad (2a)$$

$$\phi_{\check{i}}(\mathbf{r}, t) = \sum_{\check{k}\ell m} c_{\check{k}\ell m}^{\check{i}}(t) \chi_{\check{k}}(r) Y_{\ell m}(\Omega) \quad (\check{i} = \hat{M}+1, \dots, \hat{M}+\check{M}), \quad (2b)$$

restricted ansatz, but the extension to molecules with more general schemes is straightforward.

A. Space partition and FEDVR basis functions

To establish the SP concept, we follow the same strategy as in our recent work on the exterior time-scaling theory [67]. Setting the atomic nucleus at the origin of the space, let each electron exist within a spherical volume of radius r_{\max} , which is supposedly so large that the photoelectrons do not reach the end of the volume within the time interval during which the laser-induced phenomena of interest take place. Let a spherical surface Σ of radius r_Σ divide the space into two parts: the inner region \hat{V} with radial interval $0 \leq r \leq r_\Sigma$ and the outer region \check{V} with $r_\Sigma < r \leq r_{\max}$, where $\Sigma \in \hat{V}$ (see Fig. 1). The two volumes \hat{V} and \check{V} are then further subdivided into \hat{N}_{fe} and \check{N}_{fe} regions (FEs), respectively, as follows:

$$\text{Radial interval of } \hat{V}: [0, r_\Sigma] = [r_0, r_1] \cup (r_1, r_2) \cup \dots \cup (r_{\hat{N}_{\text{fe}}-1}, r_{\hat{N}_{\text{fe}}}], \quad (1a)$$

$$\text{Radial interval of } \check{V}: (r_\Sigma, r_{\max}] = (r_{\hat{N}_{\text{fe}}}, r_{\hat{N}_{\text{fe}}+1}) \cup \dots \cup (r_{\hat{N}_{\text{fe}}+\check{N}_{\text{fe}}-1}, r_{\hat{N}_{\text{fe}}+\check{N}_{\text{fe}}}], \quad (1b)$$

which satisfy the boundary conditions: $\phi_i(\mathbf{r}, t)|_{r=0} = \phi_i(\mathbf{r}, t)|_{r \geq r_\Sigma} = \phi_i(\mathbf{r}, t)|_{r \leq r_\Sigma} = \phi_i(\mathbf{r}, t)|_{r=r_{\max}} = 0$. The construction of a wave function which is continuously differentiable across Σ necessitates introducing additional TI orbitals; their radial part consists only of $\chi_b(r)$:

$$\phi_{\bar{i}}(\mathbf{r}) = \chi_b(r) Y_{\ell m}(\Omega) \quad (\bar{i} = \hat{M} + \check{M} + 1, \dots, \hat{M} + \check{M} + \bar{M}), \quad (2c)$$

where each orbital index \bar{i} corresponds to each pair of angular momentum quantum number, ℓ and m . That is, if, in a computation, taking into account $\ell = 0, \dots, \ell_{\max}$ with $m = -\ell, \dots, \ell$ for each value of ℓ , the TI orbitals are defined as follows: $\phi_{\hat{M}+\check{M}+1}(\mathbf{r}) = \chi_b(r) Y_{00}(\Omega)$, $\phi_{\hat{M}+\check{M}+2}(\mathbf{r}) = \chi_b(r) Y_{1,-1}(\Omega)$, $\phi_{\hat{M}+\check{M}+3}(\mathbf{r}) = \chi_b(r) Y_{1,0}(\Omega)$, ..., $\phi_{\hat{M}+\check{M}+\bar{M}}(\mathbf{r}) = \chi_b(r) Y_{\ell_{\max} m_{\max}}(\Omega)$, where the total number of them amounts to $\bar{M} = (\ell_{\max} + 1)^2$. The TI orbitals are important but additional ingredients, so that these are not illustrated in Fig. 1.

Then, let three single-particle Hilbert spaces consist of the TD and TI orbitals [Eq. (2c)]:

$$\hat{\mathcal{P}} \equiv \{\phi_{\hat{i}}(\mathbf{r}, t)|\hat{i} = 1, \dots, \hat{M}\}, \quad (3a)$$

$$\check{\mathcal{P}} \equiv \{\phi_{\check{i}}(\mathbf{r}, t)|\check{i} = \hat{M} + 1, \dots, \hat{M} + \check{M}\}, \quad (3b)$$

$$\bar{\mathcal{P}} \equiv \{\phi_{\bar{i}}(\mathbf{r})|\bar{i} = \hat{M} + \check{M} + 1, \dots, \hat{M} + \check{M} + \bar{M}\}. \quad (3c)$$

The complementaries to $\hat{\mathcal{P}}$ and $\check{\mathcal{P}}$ in \hat{V} and \check{V} , respectively, are then defined by

$$\hat{\mathcal{Q}} \equiv \{\chi_{\hat{k}}(r) Y_{\ell m}(\Omega)\}_{\hat{k}\ell m} \setminus \hat{\mathcal{P}} \equiv \{\phi_{\hat{a}}(\mathbf{r}, t)\}_{\hat{a}}, \quad (4a)$$

$$\check{\mathcal{Q}} \equiv \{\chi_{\check{k}}(r) Y_{\ell m}(\Omega)\}_{\check{k}\ell m} \setminus \check{\mathcal{P}} \equiv \{\phi_{\check{a}}(\mathbf{r}, t)\}_{\check{a}}, \quad (4b)$$

where the virtual orbitals, hereafter also called $\hat{\mathcal{Q}}$ - and $\check{\mathcal{Q}}$ -space orbitals, are defined by the second equivalences and abstractly

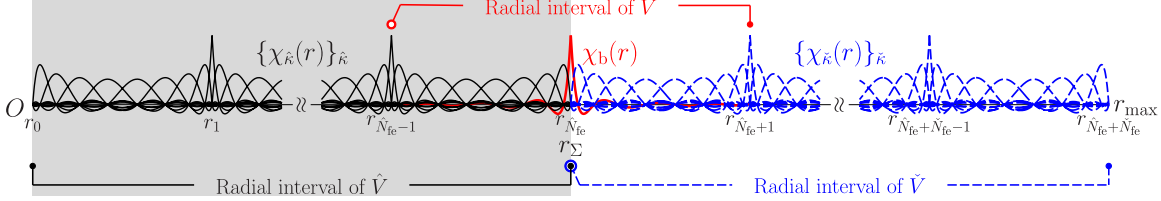


FIG. 2. Setup of the FEDVR functions in the radial coordinate. Dividing the interval $[0, r_{\max}]$ into two parts, $[0, r_{\Sigma}]$ (shaded area) and $(r_{\Sigma}, r_{\max}]$, they are further subdivided into \hat{N}_{fe} and \check{N}_{fe} intervals (FEs), respectively. Defining a set of Lobatto DVR functions with N_{dvr} quadrature points in each FE, the FEDVR functions are constructed along the standard prescription (cf. Ref. [42]). The FEDVR functions are classified into three categories, $\{\chi_{\hat{k}}(r)\}_{\hat{k}} = 1, \dots, (N_{\text{dvr}} - 1)\hat{N}_{\text{fe}} - 1\}$, $\{\chi_b(r)\} = \{\chi_{(N_{\text{dvr}} - 1)\hat{N}_{\text{fe}}} (r)\}$, and $\{\chi_{\check{k}}(r)\}_{\check{k}} = (N_{\text{dvr}} - 1)\hat{N}_{\text{fe}} + 1, \dots, (N_{\text{dvr}} - 1)(\hat{N}_{\text{fe}} + \check{N}_{\text{fe}}) - 1\}$, and illustrated by solid, thick solid (red), and dashed (blue) lines, respectively. Although the domain of every FEDVR function extends over the whole interval, $[0, r_{\max}]$, each function is explicitly illustrated only in its nonvanishing region. The three volumes \hat{V} , \check{V} , and \bar{V} are, respectively, defined such that their radial intervals are given by $[0, r_{\Sigma}]$, $(r_{\Sigma}, r_{\max}]$, and $(r_{\hat{N}_{\text{fe}}-1}, r_{\hat{N}_{\text{fe}}+1}]$.

indexed by \hat{a} and \check{a} . See, e.g., Refs. [50–53], in which one can find similar definitions of \mathcal{P} and \mathcal{Q} as a custom of the MCTDH(F) theory.

C. Notation

As have already been used thus far, the accents *hat*, “ $\hat{\cdot}$ ”, *check*, “ $\check{\cdot}$ ”, and *bar*, “ $\check{\cdot}$ ” atop symbols indicate their associations with \hat{V} , \check{V} , and \bar{V} , respectively: $\hat{\mathcal{P}}$, $\check{\mathcal{Q}}$, $\phi_i(\mathbf{r}, t)$, $\phi_{\hat{a}}(\mathbf{r}, t)$, and $\chi_{\hat{k}}(r)$ are all related to \hat{V} ; $\check{\mathcal{P}}$, $\check{\mathcal{Q}}$, $\phi_{\check{i}}(\mathbf{r}, t)$, $\phi_{\check{a}}(\mathbf{r}, t)$, and $\chi_{\check{k}}(r)$ are all defined in relation to \check{V} ; $\bar{\mathcal{P}}$ and $\phi_i(\mathbf{r})$ [and $\chi_b(r)$] are related to \bar{V} .

To avoid repeating tedious expressions in the formulation below, we introduce a simple set of rules for concise notation: Let $\hat{p}, \hat{q}, \hat{r}, \hat{s}, \dots$ ($\check{p}, \check{q}, \check{r}, \check{s}, \dots$) be the indices of orbitals belonging to either $\hat{\mathcal{P}}$ or $\check{\mathcal{Q}}$ ($\check{\mathcal{P}}$ or $\check{\mathcal{Q}}$), while $\hat{i}, \hat{j}, \hat{k}, \hat{l}, \dots$ ($\check{i}, \check{j}, \check{k}, \check{l}, \dots$) refer to $\hat{\mathcal{P}}$ ($\check{\mathcal{P}}$), and $\hat{a}, \hat{b}, \hat{c}, \hat{d}, \dots$ ($\check{a}, \check{b}, \check{c}, \check{d}, \dots$) to $\check{\mathcal{Q}}$ ($\check{\mathcal{Q}}$). A symbol with no accent means either case: \mathcal{P} stands for either $\hat{\mathcal{P}}$ or $\check{\mathcal{P}}$ or $\bar{\mathcal{P}}$; i, j, k, l, \dots stand for either $\hat{i}, \hat{j}, \hat{k}, \hat{l}, \dots$ or $\check{i}, \check{j}, \check{k}, \check{l}, \dots$ or $\bar{i}, \bar{j}, \bar{k}, \bar{l}, \dots$ or $\check{i}, \check{j}, \check{k}, \check{l}, \dots$, i.e., $\phi_i(\mathbf{r}, t)$ means either $\phi_{\hat{i}}(\mathbf{r}, t)$ or $\phi_{\check{i}}(\mathbf{r}, t)$ or $\phi_i(\mathbf{r})$ [be careful that $\phi_i(\mathbf{r}, t)$ could be time independent if it means $\phi_i(\mathbf{r})$]; a, b, c, d, \dots stand for either $\hat{a}, \hat{b}, \hat{c}, \hat{d}, \dots$ or $\check{a}, \check{b}, \check{c}, \check{d}, \dots$, i.e., $\phi_a(\mathbf{r}, t)$ means either $\phi_{\hat{a}}(\mathbf{r}, t)$ or $\phi_{\check{a}}(\mathbf{r}, t)$. The orbitals indexed by p, q, r, s, \dots represent the most general orbitals, that is to say, $\phi_p(\mathbf{r}, t)$ means either $\phi_i(\mathbf{r}, t)$ or $\phi_a(\mathbf{r}, t)$. Appendix B provides a summary of these notation rules.

D. TD-RASSCF-SP wave function

Based on the spin-restricted ansatz, let the N_e -electron wave function consist of the TD and TI orbitals [Eq. (2)] in a piecewise manner:

$$|\Psi(t)\rangle = \sum_{\gamma=0}^{\Gamma} |\Psi_{\gamma}(t)\rangle = \sum_{\gamma=0}^{\Gamma} \sum_{I_{\gamma} \in \mathcal{V}_{\gamma}} C_{I_{\gamma}}(t) |\Phi_{I_{\gamma}}(t)\rangle, \quad (5)$$

with $0 \leq \Gamma \leq N_e$ (see Fig. 1). The total wave function is expanded in terms of $|\Psi_{\gamma}(t)\rangle$, each of which is then CI expanded in a Fock subspace \mathcal{V}_{γ} with Slater determinants $|\Phi_{I_{\gamma}}(t)\rangle$ composed of the TD and TI orbitals [Eq. (2)]: $N_e - \gamma$ chosen from $\hat{\mathcal{P}}$ and γ from $\check{\mathcal{P}} \oplus \bar{\mathcal{P}}$; consequently, $N_e - \gamma$ electrons always remain in \hat{V} . See Fig. 1 and notice the difference from it due to the introduction of \check{V} and

\bar{V} . The Slater determinants are multi-indexed by I_{γ} and orthonormalized to each other, i.e., $\langle \Phi_{I_{\gamma}}(t) | \Phi_{J_{\gamma'}}(t) \rangle = \delta_{I_{\gamma}, J_{\gamma'}}$, whence the wave function is normalized as follows:

$$\langle \Psi(t) | \Psi(t) \rangle = \sum_{\gamma=0}^{\Gamma} \langle \Psi_{\gamma}(t) | \Psi_{\gamma}(t) \rangle = \sum_{\gamma=0}^{\Gamma} \sum_{I_{\gamma} \in \mathcal{V}_{\gamma}} |C_{I_{\gamma}}(t)|^2 = 1. \quad (6)$$

By setting $\Gamma = 2$, for instance, the TD-RASSCF-SP wave function [Eq. (5)] can take into account single and double ionization; Γ represents the maximum number of electrons in \hat{V} . Although accurate description of the electronic structure and dynamics in \hat{V} requires \hat{M} to be large, the computation will be kept feasible because capturing the two-electron correlation in \check{V} would require \check{M} to be not so large. Below the TD-RASSCF-SP method is formulated to deal with such multiple-ionization dynamics with minimal numerical effort upon the assumption that the values of \hat{M} and \check{M} needed to achieve good convergence are, respectively, determined by the maximum numbers of electrons in \hat{V} and \check{V} , e.g., $\hat{M} \geq N_e$ and $\check{M} \geq \Gamma$.

In the construction of each Slater determinant $|\Phi_{I_{\gamma}}(t)\rangle$, imposing some restrictions on electron excitations within $\hat{\mathcal{P}}$ will help increase numerical efficiency. For example, let $\hat{\mathcal{P}}$ be subdivided into three parts: the inactive-core space $\hat{\mathcal{P}}_0$, and the two active spaces $\hat{\mathcal{P}}_1$ and $\hat{\mathcal{P}}_2$, between which electron excitations take place with certain restrictions to reduce the number of configurations (see our previous works in Refs. [58–60]). To keep the formulation simple and mainly focus on the SP concept, however, such RAS schemes within $\hat{\mathcal{P}}$ are not considered in this paper.

III. FORMULATION

Following the preliminaries in Sec. II, this section presents the derivation of the equations of motion, i.e., the equations obeyed by the CI-expansion coefficients $\{C_{I_{\gamma}}(t)\}_{I_{\gamma}}$ and the TD orbitals $\{\phi_i(\mathbf{r}, t)\}_{i=1}^{\hat{M}+\check{M}}$. The derivation is based on the TD variational principle [68,69] and, to some extent, follows the same formulation of the TD-RASSCF theory as in Refs. [58–60]. In the interest of keeping this paper self-contained and carefully generalizing the formalism with SP, however, a detailed account of the derivation is given.

A. Formal derivation of the equations of motion

The derivation of the equations of motion commences with defining an action functional,

$$\mathcal{S}[\{C_{I_\gamma}(t)\}, \{\phi_i(t)\}, \{\varepsilon_j^i(t)\}] = \int_0^T \left\{ \langle \Psi(t) | \left[i \frac{\partial}{\partial t} - H(t) \right] | \Psi(t) \rangle + \sum_{ij} \varepsilon_j^i(t) [\langle \phi_i(t) | \phi_j(t) \rangle - \delta_j^i] \right\} dt, \quad (7)$$

where $H(t)$ is the Hamiltonian whose explicit form is given later [Eq. (16)], and $\varepsilon_j^i(t)$ are Lagrange multipliers introduced to impose orthonormality among the \mathcal{P} -space orbitals during the time interval $[0, T]$. We then apply the TD variational principle [68,69] which states that, on the manifold formed by the set of parameters, $\{C_{I_\gamma}(t)\}_{I_\gamma}$, $\{\phi_i(\mathbf{r}, t)\}_{i=1}^{\hat{M}+\check{M}}$, and $\{\varepsilon_j^i(t)\}_{i,j=1}^{\hat{M}+\check{M}}$, a stationary point of the action functional realizes an approximation of the true solution to the TD Schrödinger equation. The variation of the action functional reads

$$\begin{aligned} \delta \mathcal{S}[\{C_{I_\gamma}(t)\}, \{\phi_i(t)\}, \{\varepsilon_j^i(t)\}] = & \int_0^T \left\{ \langle \delta \Psi(t) | \left[i \frac{\partial}{\partial t} - H(t) \right] | \Psi(t) \rangle + \langle \Psi(t) | \left[-i \frac{\overleftarrow{\partial}}{\partial t} - H(t) \right] | \delta \Psi(t) \rangle \right. \\ & \left. + \sum_{ij} [\delta \varepsilon_j^i(t) [\langle \phi_i(t) | \phi_j(t) \rangle - \delta_j^i] + \varepsilon_j^i(t) [\langle \delta \phi_i(t) | \phi_j(t) \rangle + \langle \phi_i(t) | \delta \phi_j(t) \rangle]] \right\} dt, \end{aligned} \quad (8)$$

where $\langle \Psi(t) | H(t) | \Psi(t) \rangle = \langle \Psi(t) | H^\dagger(t) | \Psi(t) \rangle$ was used, and, with the end-point condition $|\delta \Psi(0)\rangle = |\delta \Psi(T)\rangle = 0$, performing integration by parts introduced a time-derivative operator with a leftward-arrow denoting its action on the bra vector.

The variation of the wave function is expressed as

$$\begin{aligned} |\delta \Psi(t)\rangle = & \sum_{\gamma=0}^{\Gamma} \sum_{I_\gamma \in \mathcal{V}_\gamma} \delta C_{I_\gamma}(t) |\Phi_{I_\gamma}(t)\rangle \\ & + \sum_{pq} E_p^q |\Psi(t)\rangle \langle \phi_p(t) | \delta \phi_q(t)\rangle, \end{aligned} \quad (9)$$

where E_p^q is the spin-free excitation operator defined by Eq. (17a) below. In Eq. (9), the orbital index pair (p, q) is either (\hat{p}, \hat{q}) or (\check{p}, \check{q}) , because of no overlap between $\phi_{\hat{p}}(\mathbf{r}, t)$ and $\phi_{\check{p}}(\mathbf{r}, t)$, and also of $\langle \phi_{\hat{i}} | \delta \phi_{\hat{j}}(t) \rangle = \langle \phi_{\check{i}} | \delta \phi_{\check{j}}(t) \rangle = 0$ and $|\delta \phi_{\hat{i}}\rangle = 0$.

It immediately follows from Eq. (8) that imposing $\delta \mathcal{S}/\delta \varepsilon_j^i = 0$ leads to

$$\langle \phi_i(t) | \phi_j(t) \rangle = \delta_j^i \quad (i, j = 1, \dots, \hat{M} + \check{M}), \quad (10)$$

ensuring the orthonormality among the \mathcal{P} -space orbitals. Next, from Eqs. (8) and (9), the stationary condition $\delta \mathcal{S}/\delta C_{I_\gamma}^* = 0$ results in a set of equations determining the time evolution of the CI-expansion coefficients,

$$i \dot{C}_{I_\gamma}(t) + \langle \Phi_{I_\gamma}(t) | [i D(t) - H(t)] | \Psi(t) \rangle = 0, \quad (11)$$

with the orbital-time-derivative operator defined by

$$D(t) = \sum_{pq} \eta_q^p(t) E_p^q = \sum_{\hat{p}\hat{q}} \eta_{\hat{q}}^{\hat{p}}(t) E_{\hat{p}}^{\hat{q}} + \sum_{\check{p}\check{q}} \eta_{\check{q}}^{\check{p}}(t) E_{\check{p}}^{\check{q}}, \quad (12)$$

where $\eta_q^p(t) = \langle \phi_p(t) | \dot{\phi}_q(t) \rangle$. Note that $\eta_{\hat{i}}^{\hat{j}}(t)$ and $\eta_{\check{i}}^{\check{j}}(t)$ can take arbitrary values in our TD-RASSCF-SP theory as shown in Sec. III B 3, and also that $\eta_j^i(t)$ is zero for the rest of index pairs; hence let $\eta_j^i(t)$ be zero for all index pairs to avoid unnecessary complications. On the other hand, the stationary condition

$\delta \mathcal{S}/\delta \phi_i$ gives a set of equations,

$$\begin{aligned} \sum_q |\phi_q(t)\rangle \langle \Psi(t) | E_i^q \left\{ i \sum_{\gamma=0}^{\Gamma} \sum_{I_\gamma \in \mathcal{V}_\gamma} \dot{C}_{I_\gamma}(t) |\Phi_{I_\gamma}(t)\rangle \right. \\ \left. + [i D(t) - H(t)] |\Psi(t)\rangle \right\} + \sum_j |\phi_j(t)\rangle \varepsilon_j^i(t) = 0, \end{aligned} \quad (13)$$

where (i, q) is either (\hat{i}, \hat{q}) or (\check{i}, \check{q}) . The solution to Eq. (13) is to be expressed as

$$\begin{aligned} |\phi_i(t)\rangle = & \sum_j |\phi_j(t)\rangle \eta_i^j(t) + Q(t) |\dot{\phi}_i(t)\rangle = Q(t) |\dot{\phi}_i(t)\rangle \\ (i = 1, \dots, \hat{M} + \check{M}), \end{aligned} \quad (14)$$

where $Q(t)$ means either $\hat{Q}(t)$ or $\check{Q}(t)$ defined as follows:

$$\hat{Q}(t) = \sum_{\hat{a}} |\phi_{\hat{a}}(t)\rangle \langle \phi_{\hat{a}}(t)| = \hat{\mathbb{1}} - \sum_{\hat{i}} |\phi_{\hat{i}}(t)\rangle \langle \phi_{\hat{i}}(t)|, \quad (15a)$$

$$\check{Q}(t) = \sum_{\check{a}} |\phi_{\check{a}}(t)\rangle \langle \phi_{\check{a}}(t)| = \check{\mathbb{1}} - \sum_{\check{i}} |\phi_{\check{i}}(t)\rangle \langle \phi_{\check{i}}(t)|, \quad (15b)$$

with $\hat{\mathbb{1}} \equiv \sum_{\hat{p}} |\phi_{\hat{p}}(t)\rangle \langle \phi_{\hat{p}}(t)| = \sum_{\hat{k}\ell m} |\chi_{\hat{k}} Y_{\ell m}\rangle \langle \chi_{\hat{k}} Y_{\ell m}|$ and $\check{\mathbb{1}} \equiv \sum_{\check{p}} |\phi_{\check{p}}(t)\rangle \langle \phi_{\check{p}}(t)| = \sum_{\check{k}\ell m} |\chi_{\check{k}} Y_{\ell m}\rangle \langle \chi_{\check{k}} Y_{\ell m}|$.

To carry out the time propagation of the wave function, one needs to compute the sets of values, $\{C_{I_\gamma}(t)\}_{I_\gamma}$ and $\{Q(t) |\dot{\phi}_i(t)\rangle\}_{i=1}^{\hat{M}+\check{M}}$, at each time step as in the MCTDHF method. The rest of this section is hence devoted to reducing Eqs. (11) and (13) into more explicit expressions suitable for numerical computation.

B. Explicit expression of the equations of motion

Employing the length gauge within the dipole approximation, the Hamiltonian governing the dynamics of an atom

interacting with light fields reads in second quantization,

$$H(t) = \sum_{pq} h_q^p(t) E_p^q + \frac{1}{2} \sum_{pqrs} v_{qs}^{pr}(t) E_{pr}^{qs}, \quad (16)$$

where the spin-free excitation operators are defined by (see, e.g., Ref. [70])

$$E_p^q = \sum_{\sigma=\uparrow,\downarrow} a_{p\sigma}^\dagger a_{q\sigma}, \quad (17a)$$

$$E_{pr}^{qs} = \sum_{\sigma=\uparrow,\downarrow} \sum_{\tau=\uparrow,\downarrow} a_{p\sigma}^\dagger a_{r\tau}^\dagger a_{s\tau} a_{q\sigma}, \quad (17b)$$

with $a_{p\sigma}$ ($a_{p\sigma}^\dagger$) being an electron annihilation (creation) operator in the spin orbital $\phi_p(\mathbf{r}, t)\sigma(s)$, and $\sigma(s) = \uparrow$ and \downarrow denoting the spin-state function. The rest of the new symbols are defined as follows: the matrix element of the one-body operator is given by

$$h_q^p(t) = u_q^p(t) + \int \phi_p^*(\mathbf{r}, t) \left[\frac{\mathbf{L}^2}{2r^2} - \frac{Z}{r} + \mathbf{F}(t) \cdot \mathbf{r} \right] \phi_q(\mathbf{r}, t) d\mathbf{r}, \quad (18a)$$

where \mathbf{L} is the orbital angular momentum operator, Z is the nuclear charge, $\mathbf{F}(t)$ is the laser electric field, and $u_q^p(t)$ denotes

$$u_q^p(t) = \frac{1}{2} \int \frac{\partial \phi_p^*(\mathbf{r}, t)}{\partial r} \frac{\partial \phi_q(\mathbf{r}, t)}{\partial r} d\mathbf{r}. \quad (18b)$$

$$\begin{aligned} i\dot{C}_{I_\gamma}(t) = & \sum_{\hat{i}\hat{j}} h_{\hat{j}}^{\hat{i}}(t) \langle \Phi_{I_\gamma}(t) | E_{\hat{i}}^{\hat{j}} | \Psi_\gamma(t) \rangle + \sum_{\bar{i}\bar{j}} h_{\bar{j}}^{\bar{i}}(t) \langle \Phi_{I_\gamma}(t) | E_{\bar{i}}^{\bar{j}} | \Psi_\gamma(t) \rangle + \sum_{\check{i}\check{j}} h_{\check{j}}^{\check{i}}(t) \langle \Phi_{I_\gamma}(t) | E_{\check{i}}^{\check{j}} | \Psi_\gamma(t) \rangle \\ & + \frac{1}{2} \sum_{\hat{i}\hat{j}\hat{k}\hat{l}} v_{\hat{j}\hat{l}}^{\hat{i}\hat{k}}(t) \langle \Phi_{I_\gamma}(t) | E_{\hat{i}\hat{k}}^{\hat{j}\hat{l}} | \Psi_\gamma(t) \rangle + \frac{1}{2} \sum_{\bar{i}\bar{j}\bar{k}\bar{l}} v_{\bar{j}\bar{l}}^{\bar{i}\bar{k}}(t) \langle \Phi_{I_\gamma}(t) | E_{\bar{i}\bar{k}}^{\bar{j}\bar{l}} | \Psi_\gamma(t) \rangle + \frac{1}{2} \sum_{\check{i}\check{j}\check{k}\check{l}} v_{\check{j}\check{l}}^{\check{i}\check{k}}(t) \langle \Phi_{I_\gamma}(t) | E_{\check{i}\check{k}}^{\check{j}\check{l}} | \Psi_\gamma(t) \rangle \\ & + \sum_{\hat{i}\hat{j}\check{k}\check{l}} v_{\hat{j}\check{l}}^{\hat{i}\check{k}}(t) \langle \Phi_{I_\gamma}(t) | E_{\hat{i}\check{k}}^{\hat{j}\check{l}} | \Psi_\gamma(t) \rangle + \sum_{\hat{i}\check{j}\bar{k}\bar{l}} v_{\check{j}\bar{l}}^{\hat{i}\bar{k}}(t) \langle \Phi_{I_\gamma}(t) | E_{\hat{i}\bar{k}}^{\check{j}\bar{l}} | \Psi_\gamma(t) \rangle + \sum_{\check{i}\bar{j}\bar{k}\bar{l}} v_{\bar{j}\bar{l}}^{\check{i}\bar{k}}(t) \langle \Phi_{I_\gamma}(t) | E_{\check{i}\bar{k}}^{\bar{j}\bar{l}} | \Psi_\gamma(t) \rangle \\ & + \sum_{\hat{i}\bar{j}} u_{\bar{j}}^{\hat{i}}(t) \langle \Phi_{I_\gamma}(t) | E_{\hat{i}}^{\bar{j}} | \Psi_{\gamma+1}(t) \rangle + \sum_{\check{i}\bar{j}} u_{\bar{j}}^{\check{i}}(t) \langle \Phi_{I_\gamma}(t) | E_{\check{i}}^{\bar{j}} | \Psi_\gamma(t) \rangle + \sum_{\bar{i}\hat{j}} u_{\hat{j}}^{\bar{i}}(t) \langle \Phi_{I_\gamma}(t) | E_{\bar{i}}^{\hat{j}} | \Psi_{\gamma-1}(t) \rangle \\ & + \sum_{\bar{i}\check{j}} u_{\check{j}}^{\bar{i}}(t) \langle \Phi_{I_\gamma}(t) | E_{\bar{i}}^{\check{j}} | \Psi_\gamma(t) \rangle, \end{aligned} \quad (21)$$

where $\gamma = 0, 1, \dots, \Gamma$, with setting $|\Psi_{-1}(t)\rangle = |\Psi_{\Gamma+1}(t)\rangle \equiv 0$, for notational convenience. The last four terms in Eq. (21) generate the coupling between electronic states of different values of γ .

2. Q-space orbital equations

We then derive the Q -space orbital equations, i.e., equations to determine the values of $\{Q(t)|\phi_i(t)\}_{i=1}^{\tilde{M}+\check{M}}$. Premultiplying Eq. (13) by a Q -space orbital bra-vector $\langle \phi_a(t) |$ gives

$$\langle \Psi(t) | E_i^a [iD(t) - H(t)] | \Psi(t) \rangle = 0. \quad (22)$$

Substituting Eqs. (12) and (16) into Eq. (22), and performing operator algebra with Wick's theorem (see, e.g.,

All the integrals in Eq. (18) are performed over the entire volume $\hat{V} \cup \check{V}$, and $h_q^p(t)$ is nonzero for index pairs $(p, q) = (\hat{p}, \hat{q}), (\check{p}, \check{q}), (\bar{i}, \bar{j}), (\check{p}, \bar{j}), (\bar{i}, \hat{q}), (\check{p}, \bar{j})$, and (\bar{i}, \check{q}) . The matrix element of the two-body operator is defined by

$$v_{qs}^{pr}(t) = \iint \phi_p^*(\mathbf{r}, t) \phi_r^*(\mathbf{r}', t) \frac{1}{|\mathbf{r} - \mathbf{r}'|} \phi_s(\mathbf{r}', t) \phi_q(\mathbf{r}, t) d\mathbf{r} d\mathbf{r}', \quad (19)$$

where each integration is performed over the entire volume and gives nonvanishing contributions in the overlapping region of each orbital pair; hence $v_{qs}^{pr}(t)$ gives nonzero values for $(p, q) = (\hat{p}, \hat{q}), (\check{p}, \check{q})$, and (\bar{i}, \bar{j}) , with $(r, s) = (\hat{r}, \hat{s}), (\check{r}, \check{s})$, and (\bar{k}, \bar{l}) .

1. Amplitude equations

Substituting Eqs. (12) and (16) into Eq. (11) leads to

$$\begin{aligned} i\dot{C}_{I_\gamma}(t) = & \sum_{ij} h_j^i(t) \langle \Phi_{I_\gamma} | E_i^j | \Psi_\gamma \rangle \\ & + \frac{1}{2} \sum_{ijkl} v_{jl}^{ik}(t) \langle \Phi_{I_\gamma} | E_{ik}^{jl} | \Psi_\gamma(t) \rangle. \end{aligned} \quad (20)$$

Collecting only nonvanishing terms, Eq. (20) is then recast into an explicit form as follows:

$$\begin{aligned} i\dot{C}_{I_\gamma}(t) = & \sum_{\hat{i}\hat{j}} h_{\hat{j}}^{\hat{i}}(t) \langle \Phi_{I_\gamma}(t) | E_{\hat{i}}^{\hat{j}} | \Psi_\gamma(t) \rangle + \sum_{\bar{i}\bar{j}} h_{\bar{j}}^{\bar{i}}(t) \langle \Phi_{I_\gamma}(t) | E_{\bar{i}}^{\bar{j}} | \Psi_\gamma(t) \rangle + \sum_{\check{i}\check{j}} h_{\check{j}}^{\check{i}}(t) \langle \Phi_{I_\gamma}(t) | E_{\check{i}}^{\check{j}} | \Psi_\gamma(t) \rangle \\ & + \frac{1}{2} \sum_{\hat{i}\hat{j}\hat{k}\hat{l}} v_{\hat{j}\hat{l}}^{\hat{i}\hat{k}}(t) \langle \Phi_{I_\gamma}(t) | E_{\hat{i}\hat{k}}^{\hat{j}\hat{l}} | \Psi_\gamma(t) \rangle + \frac{1}{2} \sum_{\bar{i}\bar{j}\bar{k}\bar{l}} v_{\bar{j}\bar{l}}^{\bar{i}\bar{k}}(t) \langle \Phi_{I_\gamma}(t) | E_{\bar{i}\bar{k}}^{\bar{j}\bar{l}} | \Psi_\gamma(t) \rangle + \frac{1}{2} \sum_{\check{i}\check{j}\check{k}\check{l}} v_{\check{j}\check{l}}^{\check{i}\check{k}}(t) \langle \Phi_{I_\gamma}(t) | E_{\check{i}\check{k}}^{\check{j}\check{l}} | \Psi_\gamma(t) \rangle \\ & + \sum_{\hat{i}\hat{j}\check{k}\check{l}} v_{\hat{j}\check{l}}^{\hat{i}\check{k}}(t) \langle \Phi_{I_\gamma}(t) | E_{\hat{i}\check{k}}^{\hat{j}\check{l}} | \Psi_\gamma(t) \rangle + \sum_{\hat{i}\check{j}\bar{k}\bar{l}} v_{\check{j}\bar{l}}^{\hat{i}\bar{k}}(t) \langle \Phi_{I_\gamma}(t) | E_{\hat{i}\bar{k}}^{\check{j}\bar{l}} | \Psi_\gamma(t) \rangle + \sum_{\check{i}\bar{j}\bar{k}\bar{l}} v_{\bar{j}\bar{l}}^{\check{i}\bar{k}}(t) \langle \Phi_{I_\gamma}(t) | E_{\check{i}\bar{k}}^{\check{j}\bar{l}} | \Psi_\gamma(t) \rangle \\ & + \sum_{\hat{i}\bar{j}} u_{\bar{j}}^{\hat{i}}(t) \langle \Phi_{I_\gamma}(t) | E_{\hat{i}}^{\bar{j}} | \Psi_{\gamma+1}(t) \rangle + \sum_{\check{i}\bar{j}} u_{\bar{j}}^{\check{i}}(t) \langle \Phi_{I_\gamma}(t) | E_{\check{i}}^{\bar{j}} | \Psi_\gamma(t) \rangle + \sum_{\bar{i}\hat{j}} u_{\hat{j}}^{\bar{i}}(t) \langle \Phi_{I_\gamma}(t) | E_{\bar{i}}^{\hat{j}} | \Psi_{\gamma-1}(t) \rangle \\ & + \sum_{\bar{i}\check{j}} u_{\check{j}}^{\bar{i}}(t) \langle \Phi_{I_\gamma}(t) | E_{\bar{i}}^{\check{j}} | \Psi_\gamma(t) \rangle, \end{aligned} \quad (21)$$

Ref. [71]),

$$E_i^a E_p^q = \sum_{\sigma\tau} a_{i\sigma}^\dagger a_{p\tau}^\dagger a_{q\tau} a_{a\sigma} + \delta_a^p E_i^q, \quad (23a)$$

$$E_i^a E_{pr}^{qs} = \sum_{\sigma\tau\upsilon} a_{i\sigma}^\dagger a_{p\tau}^\dagger a_{r\upsilon}^\dagger a_{s\upsilon} a_{q\tau} a_{a\sigma} + \delta_a^p E_{ir}^{qs} + \delta_a^r E_{ip}^{sq}, \quad (23b)$$

we obtain

$$\sum_j [i\eta_j^a(t) - h_j^a(t)] \rho_i^j - \sum_{jkl} v_{jl}^{ak}(t) \rho_{ik}^{jl}(t) = 0, \quad (24)$$

where the elements of the one- and two-electron reduced-density matrices, respectively, are defined by

$$\rho_i^j(t) = \langle \Psi(t) | E_i^j | \Psi(t) \rangle, \quad (25a)$$

$$\rho_{ik}^{jl}(t) = \langle \Psi(t) | E_{ik}^{jl} | \Psi(t) \rangle. \quad (25b)$$

Then multiply both sides of Eq. (24) by $|\phi_a(t)\rangle$ from the left. Take summation over all indices of the virtual orbitals, and use the definitions of the projection operators in Eq. (15). After these manipulations, the \mathcal{Q} -space orbital equations appear explicitly (see also Ref. [58]):

$$i \sum_{\hat{j}} \hat{Q}(t) |\dot{\phi}_{\hat{j}}(t)\rangle \rho_i^{\hat{j}}(t) = \hat{Q}(t) \left\{ \sum_{\hat{j}} \left[\rho_i^{\hat{j}}(t) h(t) + \sum_{kl} \rho_{ik}^{jl}(t) W_l^k(t) \right] |\phi_{\hat{j}}(t)\rangle + \sum_{\check{j}} u |\phi_{\check{j}}\rangle \rho_i^{\check{j}}(t) \right\}, \quad (26a)$$

$$i \sum_{\check{j}} \check{Q}(t) |\dot{\phi}_{\check{j}}(t)\rangle \rho_i^{\check{j}}(t) = \check{Q}(t) \left\{ \sum_{\check{j}} \left[\rho_i^{\check{j}}(t) h(t) + \sum_{kl} \rho_{ik}^{jl}(t) W_l^k(t) \right] |\phi_{\check{j}}(t)\rangle + \sum_{\hat{j}} u |\phi_{\hat{j}}\rangle \rho_i^{\hat{j}}(t) \right\}, \quad (26b)$$

where $h(t)$ and u are the one-body operators such that their matrix elements are defined by Eqs. (18a) and (18b), respectively, and the mean-field operator is defined by

$$W_l^k(\mathbf{r}, t) = \int \phi_k^*(\mathbf{r}', t) \frac{1}{|\mathbf{r} - \mathbf{r}'|} \phi_l(\mathbf{r}', t) d\mathbf{r}', \quad (27)$$

which gives nonzero values for index pairs $(k, l) = (\hat{k}, \hat{l}), (\check{k}, \check{l})$, and (\bar{k}, \bar{l}) . In Eq. (26b), $\sum_{kl} \rho_{ik}^{jl}(t) W_l^k(t) = \sum_{\hat{k}\hat{l}} \rho_{i\hat{k}}^{\hat{j}\hat{l}}(t) W_{\hat{l}}^{\hat{k}}(t) + \sum_{\bar{k}\bar{l}} \rho_{i\bar{k}}^{\bar{j}\bar{l}}(t) W_{\bar{l}}^{\bar{k}}(t) + \sum_{\check{k}\check{l}} \rho_{i\check{k}}^{\check{j}\check{l}}(t) W_{\check{l}}^{\check{k}}(t)$; its physical meaning is hence as follows: the first two summations indicate the screening effect, and the last one represents the electron correlation within \tilde{V} . The corresponding term in Eq. (26a) represents similar physical meaning.

3. P-space orbital equations

Finally, let us prove that $\eta_i^{\hat{j}}(t)$ and $\eta_i^{\check{j}}(t)$ can take arbitrary values in our TD-RASSCF-SP scheme. Premultiplying Eq. (13) by $\langle \phi_j(t) |$ gives

$$\begin{aligned} & \langle \Psi(t) | E_i^j [iD(t) - H(t)] | \Psi(t) \rangle \\ & + i \sum_{\gamma=0}^{\Gamma} \sum_{I_{\gamma} \in \mathcal{V}_{\gamma}} \langle \Psi_{\gamma}(t) | E_i^j | \Phi_{I_{\gamma}}(t) \rangle \dot{C}_{I_{\gamma}}(t) + \varepsilon_j^i(t) = 0. \end{aligned} \quad (28)$$

On the other hand, taking the stationary condition $\delta S / |\delta \phi_j(t)\rangle = 0$ followed by multiplication by $|\phi_i(t)\rangle$ from the right provides an equation containing the same Lagrange multiplier. Subtracting one from the other removes the multiplier and gives the \mathcal{P} -space orbital equations,

$$\begin{aligned} & \langle \Psi(t) | [iD(t) - H(t)] E_i^j | \Psi(t) \rangle \\ & - \langle \Psi(t) | E_i^j [iD(t) - H(t)] | \Psi(t) \rangle = i \dot{\rho}_i^j(t), \end{aligned} \quad (29)$$

where, because of the index pair (i, j) being either (\hat{i}, \hat{j}) or (\check{i}, \check{j}) , $\dot{\rho}_i^j(t)$ reads

$$\begin{aligned} \dot{\rho}_i^j(t) = & \sum_{\gamma=0}^{\Gamma} \sum_{I_{\gamma} \in \mathcal{V}_{\gamma}} [\dot{C}_{I_{\gamma}}^*(t) \langle \Phi_{I_{\gamma}}(t) | E_i^j | \Psi_{\gamma}(t) \rangle \\ & + \langle \Psi_{\gamma}(t) | E_i^j | \Phi_{I_{\gamma}}(t) \rangle \dot{C}_{I_{\gamma}}(t)]. \end{aligned} \quad (30)$$

Using Eqs. (11) and (30) in Eq. (29) results in

$$\begin{aligned} & \sum_{\gamma=0}^{\Gamma} [\langle \Psi | [iD(t) - H(t)] [1 - \Pi_{\gamma}(t)] E_i^j | \Psi_{\gamma}(t) \rangle \\ & - \langle \Psi_{\gamma}(t) | E_i^j [1 - \Pi_{\gamma}(t)] [iD(t) - H(t)] | \Psi(t) \rangle] = 0, \end{aligned} \quad (31)$$

with projection operators defined by

$$\Pi_{\gamma}(t) = \sum_{I_{\gamma} \in \mathcal{V}_{\gamma}} |\Phi_{I_{\gamma}}(t)\rangle \langle \Phi_{I_{\gamma}}(t)| \quad (\gamma = 0, \dots, \Gamma). \quad (32)$$

Noticing a relation,

$$[1 - \Pi_{\gamma}(t)] E_i^j | \Psi_{\gamma}(t) \rangle = \langle \Psi_{\gamma}(t) | E_i^j [1 - \Pi_{\gamma}(t)] = 0 \quad (\gamma = 0, \dots, \Gamma), \quad (33)$$

because of (i, j) being either (\hat{i}, \hat{j}) or (\check{i}, \check{j}) , clarifies that Eqs. (29) and (31) are always satisfied, i.e., these are just identities, not equations. Consequently, $\eta_i^{\hat{j}}(t)$ and $\eta_i^{\check{j}}(t)$ can take arbitrary values. In the present work, $\eta_i^j(t)$ is set to be zero for all index pairs. Finally, note that, if additional restrictions are imposed upon the electron excitations within \hat{P} as mentioned in the last paragraph of Sec. II D, Eqs. (29) and (31) are no longer identities for index pairs (\hat{i}, \hat{j}) and should thus be solved at each time step to compute the values of $\eta_i^{\hat{j}}(t)$, as in the TD-RASSCF theory without SP [58–60].

IV. NUMERICAL DEMONSTRATION

Based on the formulation in Secs. II and III, this section aims at application of the TD-RASSCF-SP method to assess its numerical performance in comparison with corresponding MCTDHF calculations. To this end, introducing two density functions as follows will help visualize many-electron dynamics in atoms: let us define the one-dimensional (1D) radial-electron density by

$$\begin{aligned} \rho(r_1, t) = & (N_e - 1)^{-1} \int \rho(r_1, r_2, t) dr_2 \\ = & N_e \int ds_1 d\Omega_1 \left(\prod_{\mu=2}^{N_e} \int dz_{\mu} \right) |\Psi(z_1, \dots, z_{N_e}, t)|^2 \\ = & \sum_{ij} \rho_i^j(t) \int \phi_i^*(\mathbf{r}_1, t) \phi_j(\mathbf{r}_1, t) d\Omega_1 \end{aligned} \quad (34a)$$

$$= \sum_{\gamma=0}^{\Gamma} \rho_{\gamma}(r_1, t), \quad (34b)$$

where $z \equiv (\mathbf{r}, s)$ is a set of spin-spatial coordinates, and

$$\rho_\gamma(r, t) = \sum_{ij} \langle \Psi_\gamma(t) | E_i^j | \Psi_\gamma(t) \rangle \int \phi_i^*(\mathbf{r}, t) \phi_j(\mathbf{r}, t) d\Omega \quad (\gamma = 0, \dots, \Gamma), \quad (34c)$$

which is hereafter called 1D partial radial-electron density. We then define the two-dimensional (2D) radial-electron density by

$$\begin{aligned} \rho(r_1, r_2, t) &= N_e(N_e - 1) \int ds_1 d\Omega_1 \int ds_2 d\Omega_2 \\ &\times \left(\prod_{\mu=3}^{N_e} \int dz_\mu \right) |\Psi(z_1, z_2, \dots, z_{N_e}, t)|^2 \\ &= \sum_{ijkl} \rho_{ik}^{jl}(t) \int \phi_i^*(\mathbf{r}_1, t) \phi_j(\mathbf{r}_1, t) d\Omega_1 \\ &\times \int \phi_k^*(\mathbf{r}_2, t) \phi_l(\mathbf{r}_2, t) d\Omega_2. \end{aligned} \quad (35)$$

The discussion below focuses on analyzing these densities for atomic beryllium ($Z = N_e = 4$) in the ground state and for its real-time evolution under linearly polarized light fields. Every calculation was carried out in the same-sized volume of radius $r_{\max} = 200$, with setting the FEDVR parameters as follows (see Fig. 2 and remember the definitions in Sec. II A): $N_{\text{dvr}} = 10$ in every FE, with $\hat{N}_{\text{fe}} + \check{N}_{\text{fe}} = 202$ in the TD-RASSCF-SP calculations, and $\hat{N}_{\text{fe}} = 200$ (and $\check{N}_{\text{fe}} = 0$ with $r_\Sigma = r_{\max} = 200$) in the MCTDHF calculations; the width of every FE is 1 except for the following four in the TD-RASSCF-SP calculations: $(r_{\hat{N}_{\text{fe}}-2}, r_{\hat{N}_{\text{fe}}-1}], (r_{\hat{N}_{\text{fe}}-1}, r_{\hat{N}_{\text{fe}}}(=r_\Sigma)],$

$(r_{\hat{N}_{\text{fe}}}, r_{\hat{N}_{\text{fe}}+1}],$ and $(r_{\hat{N}_{\text{fe}}+1}, r_{\hat{N}_{\text{fe}}+2}],$ whose widths are set equal to 0.5. Reducing the width and thereby increasing the density of the FEDVR functions around $r = r_\Sigma$ helps fill the gap of accuracy levels between the TD and TI orbitals (see the discussion in the last paragraph of Sec. IV B). The rest of the numerical conditions are common in all calculations: the angular-momentum states, $\ell = 0, 1, 2,$ and 3 with $m = 0$ (which amounts to $\check{M} = 4$ in the TD-RASSCF-SP calculations) were taken into account; setting $m = 0$ may be acceptable just for test-calculating atomic beryllium ionized by linearly polarized fields. The time propagation was carried out by the fourth-order Runge-Kutta method with time step $\Delta t = 1.5 \times 10^{-4}$. In the treatment of the Q -space orbital equations, the reduced-density matrices formed by Eq. (25a) were, following the procedure in Ref. [51], regularized with a small constant 10^{-10} to increase the numerical stability.

A. Ground state

The ground state of atomic beryllium was obtained by means of imaginary-time relaxation [72]. Figure 3(a) displays the (solid-angle-integrated) norm square of each spatial orbital in the TD-RASSCF-SP($\hat{M} = 6, \check{M} = 3; \Gamma = 2; r_\Sigma = 30$) computation. Each has its own shape and hence looks as if each is independent of the others. Although it is hard to imagine how these orbitals construct the wave function to be smooth across the inner and outer regions, it is ensured by the present formalism. Figure 3(b) displays the 1D partial radial-electron densities $\rho_\gamma(r, t = 0)$ for $\gamma = 0, \dots, \Gamma(=2)$ [see Eq. (34c)], showing smooth connections between $\rho_\gamma(r, 0)$ and $\rho_{\gamma+1}(r, 0)$ across $r(=r_\Sigma) = 30$ (see the discussion in the last paragraph in Sec. V B). As a result, and because of Eq. (34b), the

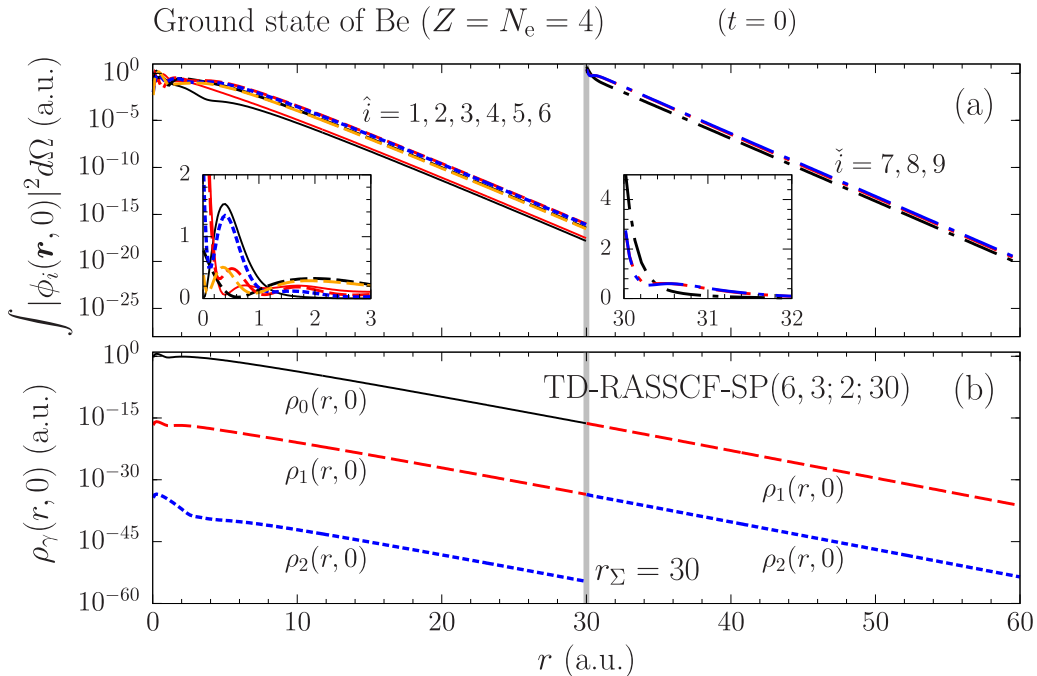


FIG. 3. (a) Plot of $|\phi_i(\mathbf{r}, t = 0)|^2$ ($i = \hat{i} = 1, \dots, 6$ and $i = \check{i} = 7, 8, 9$) after integration over the solid angles; (b) plot of the 1D partial radial-electron density $\rho_\gamma(r, t = 0)$ with $\gamma = 0, 1,$ and $2(=\Gamma)$ of atomic beryllium ($Z = N_e = 4$) in the ground state (at $t = 0$, i.e., before the interaction with light fields) computed by the TD-RASSCF-SP($\hat{M} = 6, \check{M} = 3; \Gamma = 2; r_\Sigma = 30$) method. Thick gray line along $r = r_\Sigma = 30$ indicates the position of Σ in the radial interval. The insets in (a) show zoom-ins on regions around the origin and above $r = 30$.

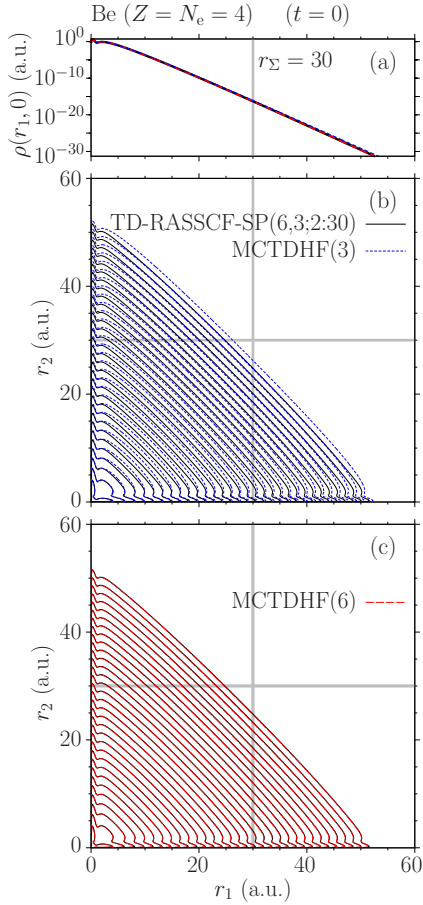


FIG. 4. (a) Plot of the 1D radial-electron density $\rho(r_1, t = 0)$; (b) and (c) contour plot of the 2D radial-electron density $\rho(r_1, r_2, t = 0)$ of atomic beryllium ($Z = N_e = 4$) in the ground state (at $t = 0$, i.e., before the interaction with light fields). Solid lines show the results of the same TD-RASSCF-SP($\tilde{M} = 6, \tilde{M}' = 3; \Gamma = 2; r_\Sigma = 30$) calculation as in Fig. 3; dotted (blue) and dashed (red) lines, respectively, represent the MCTDHF($M = 3$) and ($M = 6$) results. The contours in (b) and (c) differ by a factor of 10, decreasing outward with the innermost lines indicating 1. For comparison, both panels contain the same TD-RASSCF-SP($6,3;2;30$) result. Thick gray lines along $r_1 = 30$ and $r_2 = 30$ indicate the position of Σ in the radial interval in the TD-RASSCF-SP($6,3;2;30$) calculation. See the main text for the details of the numerical conditions used in the computations.

1D radial-electron density $\rho(r, t = 0)$ in Fig. 4(a) smoothly continues across $r = 30$. The 2D radial-electron density in Fig. 4(b) is also smooth across the boundaries along $r_1 = 30$ and $r_2 = 30$.

For comparison, Fig. 4 also shows the MCTDHF($M = 3$ and 6) results. The 1D radial-electron densities computed by the three methods are all in good agreement, but the 2D radial-electron density computed by the MCTDHF(3) method obviously differ from the other two, indicating that setting $M = 3$ is inadequate. On the other hand, the TD-RASSCF-SP($6,3;2;30$) and MCTDHF(6) calculations give almost identical 2D radial-electron density over the whole region despite the use of different numbers of orbitals in the region of $r > 30$. For a more quantitative comparison, note the values of

TABLE I. Ground-state energy (in atomic units) of atomic beryllium ($Z = N_e = 4$) computed by the MCTDHF(M) and TD-RASSCF-SP($\tilde{M}, \tilde{M}'; \Gamma; r_\Sigma$) methods. The number of the electronic configurations, i.e., $\dim \mathcal{V}$, in each calculation is listed in the third column. Because of taking only into account the angular-momentum states, $\ell = 0, 1, 2$, and 3 with $m = 0$, the values of the ground-state energy in this list are not so accurate (see, e.g., Ref. [40] for more accurate computations of the ground-state energy). See the main text for the details of the numerical conditions used in the computations.

	Method	Ground-state energy	$\dim \mathcal{V}$
MCTDHF	(3)	-14.58716	9
	(6)	-14.61559	225
TD-RASSCF-SP	(6,3;1;30)	-14.61651	1485
	(6,3;2;30)	-14.61651	3879
	(6,3;3;30)	-14.61651	5643

the ground-state energy, $\langle \Psi(0) | H(0) | \Psi(0) \rangle$, listed in Table I: the MCTDHF(6) and TD-RASSCF-SP($6,3;2;30$) methods give very close energy values, but the MCTDHF(3) result is far from them. The agreement between the MCTDHF(6) and TD-RASSCF-SP($6,3;2;30$) results seems satisfactory despite that the two theories are based on totally different variational parameters. Table I also lists the energy values computed by the TD-RASSCF-SP($6,3;1;30$) and ($6,3;3;30$) methods. The three TD-RASSCF-SP methods provide the same ground-state energy within seven digits. In Table I, note that the numbers of the electronic configurations in the TD-RASSCF-SP methods are larger than those in the MCTDHF methods. Within this level, however, there is no significant difference in computational effort between them in the treatment of the amplitude equations [Eq. (21)] and in the computation of the reduced-density matrices [Eq. (25)]. The major difference between the TD-RASSCF-SP and MCTDHF calculations comes from the treatment of the Q -space orbital equations [Eq. (26)]. Hence the numerical cost in the TD-RASSCF-SP($6,3; \Gamma = 1 \text{ or } 2 \text{ or } 3; 30$) calculation is slightly larger than in the MCTDHF(3) calculation, and yet for the present set of computational parameters, i.e., setup of the FEDVR basis functions and the value of time step, reduces to about half compared with the MCTDHF(6) calculation in terms of memory and CPU time.

The comparison among the several different MCDHF and TD-RASSCF-SP methods above clarifies the importance of using many orbitals around the nucleus for taking into account the strong correlation among all electrons, and the unnecessary of deploying such a large effort outside $\Sigma = 30$. This is exactly the assumption which motivated us to formulate the TD-RASSCF-SP theory. In the next subsection, we further look into this point in real-time evolution of atomic beryllium under strong light fields.

B. Photoionization dynamics

After the preparation of atomic beryllium in the ground state, let it real-time evolve under strong light fields. Let a laser pulse linearly polarized along the z axis be defined by its

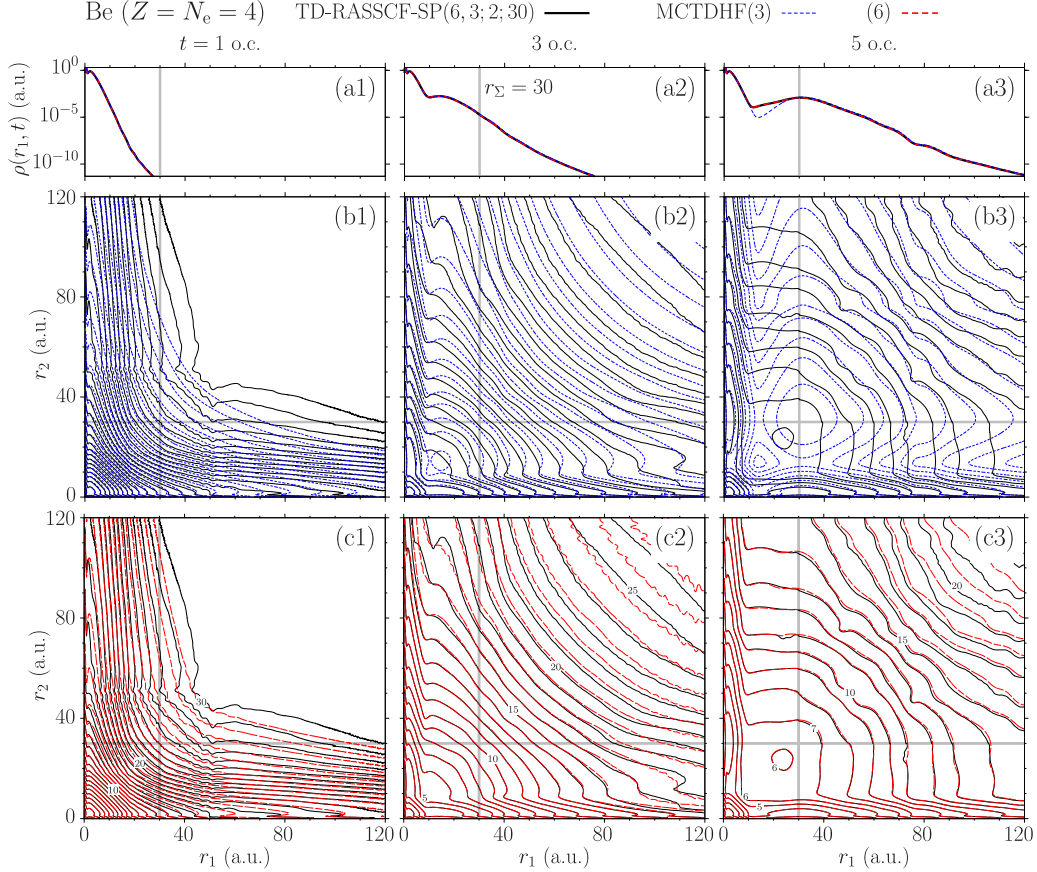


FIG. 5. Same format as Fig. 4 except that each column shows snapshots of the radial-electron densities at the first, third (just after the end of the laser pulse), and fifth optical cycle (o.c.), i.e., $t = (2\pi/\omega) \times n = 10.34n$ with $n = 1, 3$, and 5 . The three panels (c1)–(3) show the values of $-\log_{10} \rho(r_1, r_2, t)$ at several selected points on the TD-RASSCF-SP(6,3;2;30) results. See Fig. 4 and its caption.

electric field $\mathbf{F}(t) = (0, 0, -dA(t)/dt)^T$, where

$$A(t) = \begin{cases} \frac{F_0}{\omega} \sin^2\left(\frac{\pi t}{T}\right) \sin(\omega t) & (0 \leq t \leq T), \\ 0 & (T < t), \end{cases} \quad (36)$$

with electric-field strength $F_0 = 0.05338$ ($\Leftrightarrow I = 10^{14}$ W/cm 2), angular frequency $\omega = 0.6075$ ($\Leftrightarrow \lambda = 75$ nm), and pulse duration $T = 2\pi N/\omega = 10.34 \times N = 31.03$ ($N = 3$ cycles). This laser pulse can double-ionize atomic beryllium when it absorbs two photons nonsequentially. To avoid reflection of high-energy electron wave packets from the boundary of the volume ($r = r_{\max}$), a complex absorbing potential function $-iW(r)$ was added to the one-body operator $h(t)$, where $W(r) = 1 - \cos\{\pi(r - r_{\text{cap}})/[2(r_{\max} - r_{\text{cap}})]\}$ for $r > r_{\text{cap}} = 170$ and zero elsewhere [73].

Figure 5 follows Fig. 4 and shows snapshots of the time evolution of the 1D and 2D radial-electron densities at the first, third (just after the end of the pulse), and fifth optical cycles (o.c.), i.e., at $t = (2\pi/\omega) \times n = 10.34n$ with $n = 1, 3$, and 5 . The 1D radial-electron densities computed by the three methods are all in good agreement at $t = 1$ and 3 o.c. [Figs. 5(a1) and 5(a2)]. However, the MCTDHF(3) result then deviates from the other two at 5 o.c. [Fig. 5(a3)]. To understand more details, compare the 2D radial-electron densities in Figs. 5(b3) and 5(c3). The MCTDHF(3) result

largely differs from the others in the region of $0 < r_1 < 30$ and $0 < r_2 < 30$, indicating failure in capturing the electronic structure of the excited ion. The underestimation of the energy stored in the ion then seems to be reflected in overestimating the kinetic energy of the two-electron wave packet which goes outward too fast and spreads too broadly in the region of $r_1 > 30$ and $r_2 > 30$. On the other hand, comparison between the TD-RASSCF-SP(6,3;2;30) and MCTDHF(6) results in Figs. 5(c1)–5(c3) indicates the success of the SP strategy. The TD-RASSCF-SP(6,3;2;30) calculation captures well the dynamics of the core electrons as well as that of the photoelectrons.

In obtaining these results, the convergence with respect to the numerical parameters were carefully checked; the MCTDHF(M) calculation achieves qualitatively satisfactory results already for $M = 4$ and results of good accuracy for $M \geq 6$. As an illustrative comparison, Figs. 4 and 5 hence focus on the MCTDHF(3) and (6) methods and, as their hybrid, the TD-RASSCF-SP(6,3;2;30) method. As mentioned in Sec. IV A, the TD-RASSCF-SP(6,3;2;30) method requires only slightly more numerical cost than the MCTDHF(3) method, and about half the cost compared with the MCTDHF(6) method. Despite this large reduction of numerical effort, the TD-RASSCF-SP(6,3;2;30) method is comparable in accuracy to the MCTDHF(6) method in the description of the double-ionization dynamics.

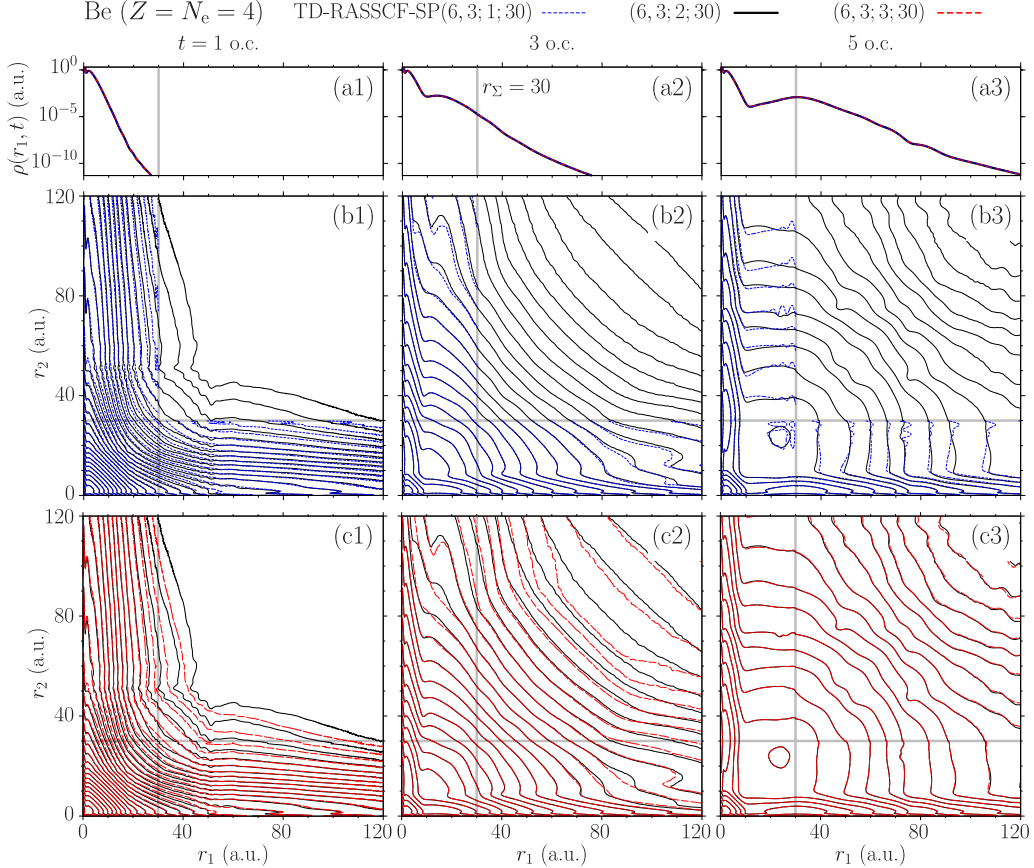


FIG. 6. Same format as Fig. 5 except giving a comparison among the TD-RASSCF-SP results computed with three different sets of parameters, $(\hat{M}, \check{M}; \Gamma; r_\Sigma) = (6, 3; 1; 30), (6, 3; 2; 30)$, and $(6, 3; 3; 30)$, respectively, represented by dotted (blue), solid, and dashed (red) lines. The TD-RASSCF-SP($6, 3; 2; 30$) results are the same as in Fig. 5, and are meant to be the reference for comparison.

Now turn to Fig. 6 which compares three different TD-RASSCF-SP calculations carried out with $(\hat{M}, \check{M}; \Gamma; r_\Sigma) = (6, 3; 1; 30), (6, 3; 2; 30)$, and $(6, 3; 3; 30)$. As clearly seen in Fig. 6(b3), the TD-RASSCF-SP($6, 3; 1; 30$) calculation creates noticeable interference structures in the 2D radial-electron density. This is expected; when the slow two-electron wave packet approaches Σ , one of the two electrons is reflected since only one electron is allowed to go through the surface. Similarly two-electron wave packet reflections were observed in an RMT computation for atomic helium in double-ionization by nonsequential two-photon absorption [27]. On the other hand, such reflections are not observed when setting $\Gamma = 2$ or 3. The very good agreement between the TD-RASSCF-SP($6, 3; 2; 30$) and $(6, 3; 3; 30)$ indicates that there hardly exists a third electron in \check{V} , and that setting $\Gamma = 2$ is enough in this laser condition. Then also look at Fig. 7, which compares the TD-RASSCF-SP($6, 3; 2; 20$), $(6, 3; 2; 30)$, and $(6, 3; 2; 40)$ results. The good agreement of the three results shows the insensitivity of the calculation with respect to the value of r_Σ around 20–40 when setting $\Gamma = 2$. However, still small differences appear, indicating the difficulty to achieve complete convergence in the description of two-electron continua.

Finally, remember that all the TD-RASSCF-SP results shown above were obtained with deploying FEDVR functions with twice the density around $r = r_\Sigma$ compared with the density in the rest of the radial interval. If every FE has equal

width 1, the 2D radial-electron density is less smooth across the lines of $r_1 = r_\Sigma$ and $r_2 = r_\Sigma$ (not shown), although the 1D radial-electron density remains smooth on the scale in Figs. 4–7. The gap of accuracy levels between the TD and TI orbitals will be the main cause for the lack of smoothness. The wave function is very accurately described on Σ where it is full-CI expanded with respect to the TI orbitals (i.e., elementary basis functions). In the rest of the volume, however, the wave function is approximated by the SCF scheme with TD orbitals. The abrupt change in the accuracy on Σ may cause some reflections, resulting in less-smoothness in the 2D radial-electron density. Reducing the width of FEs on the both sides of r_Σ is necessary to reduce this accuracy gap. However, deploying the FEDVR functions so densely makes the Q -space orbital equations stiff and necessitates setting the time step very small ($\Delta t = 1.5 \times 10^{-4}$) in the time propagation. On the other hand, the MCTDHF(3) and (6) methods can achieve convergence with a larger time step, say, $\Delta t = 5.0 \times 10^{-4}$. Hence the numerical experiments presented in this section allow us to conclude as follows: although the TD-RASSCF-SP method succeeds in increasing the numerical efficiency by setting \check{M} small while keeping reasonable accuracy, this gain is swallowed up by the use of a small time step. The solution of the stiffness problem is a challenge for making the TD-RASSCF-SP method truly efficient compared with the MCTDHF and TD-RASSCF (without SP) methods.

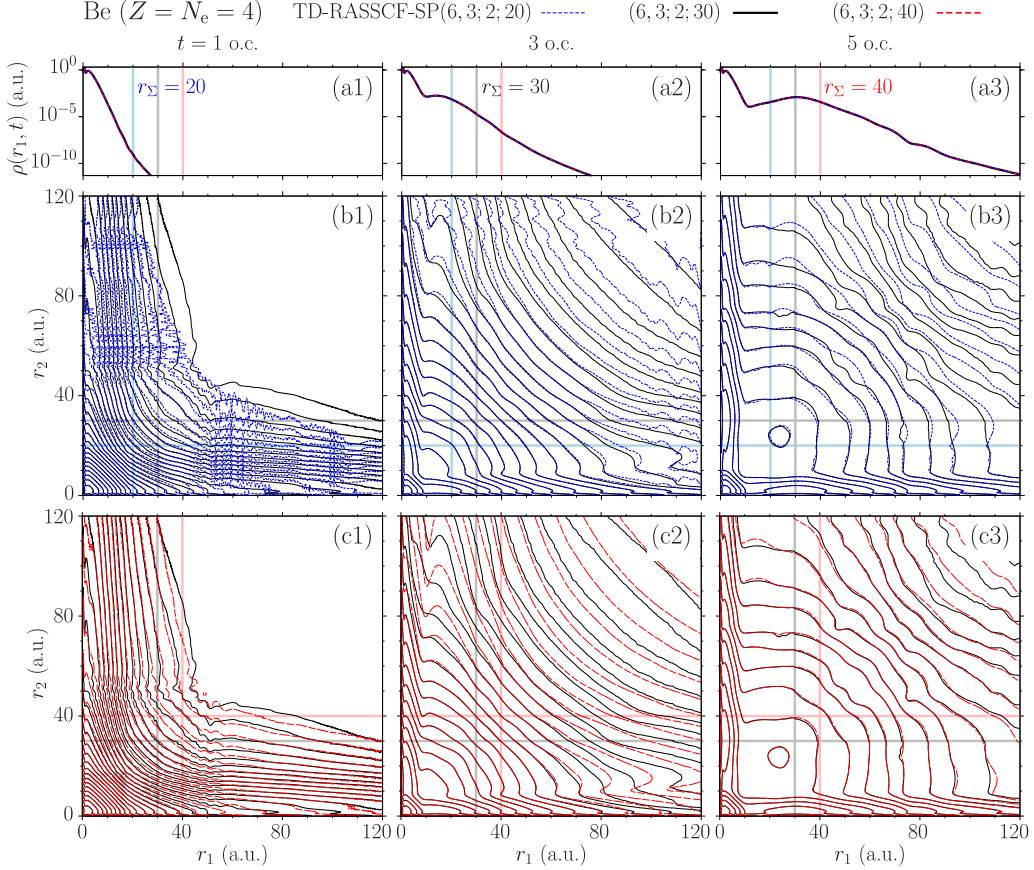


FIG. 7. Same format as Fig. 5 except giving a comparison among the TD-RASSCF-SP results computed with three different sets of parameters, $(\hat{M}, \check{M}; \Gamma; r_\Sigma) = (6,3;2;20), (6,3;2;30)$, and $(6,3;2;40)$, respectively, represented by dotted (blue), solid, and dashed (red) lines. Thick light-blue lines along $r_1 = 20$ and $r_2 = 20$, and thick pink lines along $r_1 = 40$ and $r_2 = 40$, respectively, indicate the position of Σ in the radial interval in the TD-RASSCF-SP(6,3;2;20) and (6,3;2;40) calculations. The TD-RASSCF-SP(6,3;2;30) results are the same as in Figs. 5 and 6, and are meant to be the reference for comparison.

V. DISCUSSION: BLOCH OPERATOR-BASED FORMALISM

The formulation in Secs. II and III is underpinned by the introduction of the three kinds of orbitals defined with the FEDVR basis functions. One may, however, wonder if the formulation necessitates the vanishing of the TD orbitals on Σ [Eqs. (2a) and (2b)] and the introduction of the TI orbitals whose radial part only consists of $\chi_b(r)$ [Eq. (2c)]. Getting back to basics, this section focuses on the theoretical details, and is, to this end, devoted to providing another formulation of the TD-RASSCF-SP theory in a more general manner following the original concept illustrated in Fig. 1. The Bloch operator in second quantization plays a key role in the discussion below. Then, one will see a fundamental difficulty inherent in this general formulation and hence notice the need to construct the theory as in Secs. II and III.

Without introducing the TI orbitals, let the wave function only consist of two sets of TD orbitals:

$$\phi_i(\mathbf{r}, t) = \sum_{\ell m} \left[\sum_{\tilde{\kappa}} \hat{c}_{\tilde{\kappa} \ell m}(t) \chi_{\tilde{\kappa}}(r) + \hat{c}_{\ell m}(t) \hat{\chi}_b(r) \right] Y_{\ell m}(\Omega) \quad (37a)$$

$$[\hat{i} = 1, \dots, \hat{M} (\geq N_e/2)],$$

$$\phi_i(\mathbf{r}, t) = \sum_{\ell m} \left[\sum_{\tilde{\kappa}} \hat{c}_{\tilde{\kappa} \ell m}(t) \chi_{\tilde{\kappa}}(r) + \hat{c}_{\ell m}(t) \hat{\chi}_b(r) \right] Y_{\ell m}(\Omega) \quad (37b)$$

$$[\check{i} = \hat{M} + 1, \dots, \hat{M} + \check{M}],$$

which, respectively, correspond to Eqs. (2a) and (2b), but now containing parts of the bridge function defined as follows: $\hat{\chi}_b(r) \equiv \sqrt{2} \chi_b(r)$ for $r \leq r_\Sigma$ and 0 otherwise; $\check{\chi}_b(r) \equiv \sqrt{2} \chi_b(r)$ for $r > r_\Sigma$ and 0 otherwise [see Eq. (B3) in Appendix B]. Importantly, the TD orbitals in Eq. (37) satisfy $\phi_i(\mathbf{r}, t)|_{r=0} = \phi_i(\mathbf{r}, t)|_{r>r_\Sigma} = \phi_i(\mathbf{r}, t)|_{r<r_\Sigma} = \phi_i(\mathbf{r}, t)|_{r=r_{\max}} = 0$, but their behavior on Σ is undetermined yet and needs to be specified appropriately.

Because the TI orbitals are now absent, $\check{\mathcal{P}}$ is empty, i.e., $\check{M} = 0$. On the other hand, the TD orbitals defined by Eqs. (37a) and (37b) span $\hat{\mathcal{P}}$ and $\check{\mathcal{P}}$, respectively [see Eqs. (3a) and (3b)]. Their supplementaries are $\hat{\mathcal{Q}}$ and $\check{\mathcal{Q}}$, respectively [see Eqs. (4a) and (4b)]; the projection operators, $\hat{Q}(t)$ and $\check{Q}(t)$, are now similar to those in Eqs. (15a) and (15b), but with the closure identities defined as follows: $\hat{1} \equiv \sum_{\tilde{\rho}} |\phi_{\tilde{\rho}}(t)\rangle \langle \phi_{\tilde{\rho}}(t)| = \sum_{\tilde{\kappa} \ell m} |\chi_{\tilde{\kappa}} Y_{\ell m}\rangle \langle \chi_{\tilde{\kappa}} Y_{\ell m}| + |\hat{\chi}_b Y_{\ell m}\rangle \langle \hat{\chi}_b Y_{\ell m}|$ and $\check{1} \equiv \sum_{\tilde{\rho}} |\phi_{\tilde{\rho}}(t)\rangle \langle \phi_{\tilde{\rho}}(t)| = \sum_{\tilde{\kappa} \ell m} |\chi_{\tilde{\kappa}} Y_{\ell m}\rangle \langle \chi_{\tilde{\kappa}} Y_{\ell m}| + |\check{\chi}_b Y_{\ell m}\rangle \langle \check{\chi}_b Y_{\ell m}|$. Except for these minor changes of meanings in some

symbols, the discussion below uses the same notations as in Secs. II and III, unless otherwise mentioned, to ease the comparison between the two formalisms.

Generally speaking, the orbitals can be defined with any elementary basis functions: grids, B splines, Legendre, or other DVR functions, for instance. Different sets of basis functions can also be employed in the inner and outer regions. To avoid unnecessary confusion and notational complications, however, the same FEDVR functions are employed in the description of the radial motion of each electron. The discussion below just gives some key notions in the Bloch operator-based formalism. Appendix A accounts for the detailed derivation of the equations of motion.

A. Hamiltonian and Bloch operator in second quantization

Introducing a field operator as follows helps systematically formulate the theory:

$$\begin{aligned} \Psi(z, t) &= \frac{1}{r} \sum_p \sum_{\sigma=\uparrow,\downarrow} \phi_p(\mathbf{r}, t) \sigma(s) a_{p\sigma} \\ &= \frac{1}{r} \sum_{\sigma=\uparrow,\downarrow} \sigma(s) \left[\sum_{\hat{p}} \phi_{\hat{p}}(\mathbf{r}, t) a_{\hat{p}\sigma} + \sum_{\check{p}} \phi_{\check{p}}(\mathbf{r}, t) a_{\check{p}\sigma} \right]. \end{aligned} \quad (38)$$

The Hamiltonian governing the dynamics of an atom interacting with light fields then reads in terms of the field operator (see, e.g., Ref. [74])

$$\begin{aligned} H(t) &\equiv \int \Psi^\dagger(z, t) \left[-\frac{1}{2} \Delta - \frac{Z}{r} + \mathbf{F}(t) \cdot \mathbf{r} \right] \Psi(z, t) dz \\ &+ \iint \Psi^\dagger(z, t) \Psi^\dagger(z', t) \frac{1}{|\mathbf{r} - \mathbf{r}'|} \Psi(z', t) \Psi(z, t) dz dz' \\ &\equiv \mathcal{H}(t) - \mathcal{L}(t), \end{aligned} \quad (39)$$

where $\mathcal{H}(t)$ acts on $|\Psi(t)\rangle$ as a Hermitian operator in both \hat{V} and \check{V} . On the other hand, $\mathcal{L}(t)$, stemming from Σ , is non-Hermitian in either volume, and is given by

$$\mathcal{L}(t) = \sum_{\hat{p}\hat{q}} \mathcal{L}_{\hat{q}}^{\hat{p}}(t) E_{\hat{p}}^{\hat{q}} - \sum_{\check{p}\check{q}} \mathcal{L}_{\check{q}}^{\check{p}}(t) E_{\check{p}}^{\check{q}}, \quad (40)$$

with the so-called Bloch operator \mathcal{L} [29] defined such that its matrix elements are given by

$$\mathcal{L}_{\hat{q}}^{\hat{p}}(t) = \frac{1}{2} \int d\Omega \left[\phi_{\hat{p}}^*(\mathbf{r}, t) \frac{\partial}{\partial r} \phi_{\hat{q}}(\mathbf{r}, t) \right]_{r=r_\Sigma}, \quad (41a)$$

$$\mathcal{L}_{\check{q}}^{\check{p}}(t) = \frac{1}{2} \int d\Omega \left[\phi_{\check{p}}^*(\mathbf{r}, t) \frac{\partial}{\partial r} \phi_{\check{q}}(\mathbf{r}, t) \right]_{r=r_\Sigma+0}. \quad (41b)$$

In obtaining Eq. (39), each integration with respect to r is decomposed into two parts: $\int_0^{r_{\max}} = \int_0^{r_\Sigma} + \int_{r_\Sigma+0}^{r_{\max}}$, in each of which integrating by parts gives each of Eqs. (41a) and (41b). Although the Bloch operator is usually given by a compact expression, $\frac{1}{2} \delta(r - r_\Sigma) \partial/\partial r$, this latter definition in terms of the delta function should be avoided to keep the formulation

clear; remember throughout this paper $\Sigma \in \hat{V}$. Also note that the explicit expression of $\mathcal{H}(t)$ is given by a form similar to $H(t)$ in Eq. (16), but now each integration in computing the matrix elements corresponding to Eqs. (18a), (18b), and (19) is performed in either \hat{V} or \check{V} .

B. Matching the wave function on Σ

The matching condition on Σ , i.e., the set of boundary conditions ensuring that the wave function is continuously differentiable across Σ reads

$$\Psi(z_1, \dots, z_{N_e}, t)|_{r_v=r_\Sigma} = \Psi(z_1, \dots, z_{N_e}, t)|_{r_v=r_\Sigma+0}, \quad (42a)$$

$$\frac{\partial}{\partial r_v} \Psi(z_1, \dots, z_{N_e}, t)|_{r_v=r_\Sigma} = \frac{\partial}{\partial r_v} \Psi(z_1, \dots, z_{N_e}, t)|_{r_v=r_\Sigma+0}, \quad (42b)$$

where r_v is a radial coordinate arbitrarily chosen from the N_e possible ones, $\{r_\mu\}_{\mu=1}^{N_e}$, and the coordinate representation of the wave function reads (see, e.g., Ref. [74])

$$\Psi(z_1, \dots, z_{N_e}, t) = \frac{1}{\sqrt{N_e!}} \langle \text{vac} | \left[\prod_{\mu=1}^{N_e} \Psi(z_\mu, t) \right] | \Psi(t) \rangle, \quad (43)$$

with $\langle \text{vac} |$ denoting a bra vector of the vacuum, or zero-electron state. Now express both sides of Eq. (42a) with Eq. (43), and consider a case in which among the $N_e - 1$ radial coordinates, $\{r_\mu\}_{\mu \neq v}^{N_e}$, v of them are greater than r_Σ . A manipulation involving Eq. (5) then leads to

$$\begin{aligned} \langle \text{vac} | \left[\prod_{\mu \neq v}^{N_e} \Psi(z_\mu, t) \right] &\left[\Psi(z_v, t)|_{r_v=r_\Sigma} | \Psi_\gamma(t) \rangle \right. \\ &\left. - \Psi(z_v, t)|_{r_v=r_\Sigma+0} | \Psi_{\gamma+1}(t) \rangle \right] = 0, \end{aligned} \quad (44)$$

where $\gamma = 0, \dots, \Gamma$, with $|\Psi_{\Gamma+1}(t)\rangle \equiv 0$. A calculation with Eq. (42b) in the same vein leads to an equation similar to Eq. (44) but with derivative operators. It follows from these results that the matching conditions in first quantization [Eq. (42)] are transformed to second quantization as follows:

$$\Psi(z, t)|_{r=r_\Sigma} |\Psi_\gamma(t)\rangle = \Psi(z, t)|_{r=r_\Sigma+0} |\Psi_{\gamma+1}(t)\rangle, \quad (45a)$$

$$\frac{\partial}{\partial r} \Psi(z, t)|_{r=r_\Sigma} |\Psi_\gamma(t)\rangle = \frac{\partial}{\partial r} \Psi(z, t)|_{r=r_\Sigma+0} |\Psi_{\gamma+1}(t)\rangle. \quad (45b)$$

The number of the conditions (45) is only determined by Γ , and is independent of \hat{M} and \check{M} . Compare with the usual ansatz of the R -matrix theory; each channel (ionic state) component of the wave function is subject to a matching condition (see, e.g., Refs. [12,13]). We will come back to this point in Sec. VD.

Note that the norm square of $\Psi(z, t)|\Psi_\gamma(t)\rangle$ followed by integration with respect to s and Ω gives the 1D partial

radial-electron density $\rho_\gamma(r, t)$ defined by Eq. (34c). Hence Eq. (45a) leads to a relation: $\rho_\gamma(r_\Sigma, t) = \rho_{\gamma+1}(r_\Sigma + 0, t)$. Likewise, Eqs. (45a) and (45b) lead to $\partial\rho_\gamma(r, t)/\partial r|_{r=r_\Sigma} = \partial\rho_{\gamma+1}(r, t)/\partial r|_{r=r_\Sigma+0}$. Remember Fig. 3(b), which has already indicated these relations; because the formulation in Secs. II and III employs the TI orbitals, the matching condition of the wave function on Σ is ensured from the outset.

C. Hermiticity of the total Hamiltonian

Equation (45) specifies the action of $\mathcal{L}(t)$ on $|\Psi(t)\rangle$ and hence ensures the Hermiticity of $H(t)$ with respect to $|\Psi(t)\rangle$. To make this point clear, premultiplying both sides of Eq. (45b)

$$\begin{aligned} \langle\Psi(t)|\mathcal{L}(t)|\Psi(t)\rangle &= \sum_{\gamma=0}^{\Gamma} \left[\sum_{\hat{i}\hat{j}} \langle\Psi_\gamma(t)|E_{\hat{i}}^{\hat{j}}|\Psi_\gamma(t)\rangle \mathcal{L}_{\hat{j}}^{\hat{i}}(t) - \sum_{i\check{j}} \langle\Psi_\gamma(t)|E_i^{\check{j}}|\Psi_\gamma(t)\rangle \mathcal{L}_{\check{j}}^i(t) \right] \\ &= \sum_{\gamma=0}^{\Gamma-1} \left[\sum_{\hat{i}\hat{j}} \langle\Psi_\gamma(t)|E_{\hat{i}}^{\hat{j}}|\Psi_\gamma(t)\rangle \mathcal{L}_{\hat{j}}^{\hat{i}}(t) - \sum_{i\check{j}} \langle\Psi_{\gamma+1}(t)|E_i^{\check{j}}|\Psi_{\gamma+1}(t)\rangle \mathcal{L}_{\check{j}}^i(t) \right] + \sum_{\hat{i}\hat{j}} \langle\Psi_\Gamma(t)|E_{\hat{i}}^{\hat{j}}|\Psi_\Gamma(t)\rangle \mathcal{L}_{\hat{j}}^{\hat{i}}(t) \\ &= 0, \end{aligned} \quad (47)$$

where $\langle\Psi_0(t)|E_{\check{i}}^{\check{j}}|\Psi_0(t)\rangle = 0$ was used in obtaining the second equivalence. The expectation value of $H(t)$ [Eq. (39)] is hence written as

$$\langle\Psi(t)|H(t)|\Psi(t)\rangle = \langle\Psi(t)|\mathcal{H}(t)|\Psi(t)\rangle = \langle\Psi(t)|H^\dagger(t)|\Psi(t)\rangle, \quad (48)$$

which ensures the TD-RASSCF-SP theory to be built upon the TD variational principle. In other words, when the formulation commences with the TD variational principle assuming Eq. (48), the action of $\mathcal{L}(t)$ on $|\Psi(t)\rangle$ is implicitly specified by Eq. (45). Although Eq. (47) is satisfied, its variation gives nonzero, i.e., $\langle\delta\Psi(t)|\mathcal{L}(t)|\Psi(t)\rangle \neq 0$, so that $\mathcal{L}(t)$ appears in the formulation. See Appendix A in which the equations of motion are derived and listed for comparison to the formulation in Sec. III.

D. Boundary conditions on Σ to determine the \mathcal{P} -space orbitals

In this Bloch operator-based formalism, every \mathcal{P} -space orbital defined by Eq. (37) vanishes at the origin ($r = 0$) and at the end of the volume ($r = r_{\max}$), while it is undefined how it behaves on Σ . Hence, determining the $\hat{\mathcal{P}}$ ($\check{\mathcal{P}}$)-space orbitals at each time step by solving the $\hat{\mathcal{Q}}$ ($\check{\mathcal{Q}}$)-space orbital equations [Eq. (A9)] requires \hat{M} (\check{M}) boundary conditions on Σ . On the other hand, Eq. (46a) provides Γ boundary conditions for both the $\hat{\mathcal{P}}$ - and $\check{\mathcal{P}}$ -space orbitals, and Eq. (46b) provides $\delta_\Gamma^{N_e}$ boundary condition to the $\check{\mathcal{P}}$ -space orbitals. Hence the \mathcal{P} -space orbitals are not fully determined unless $\hat{M} - \delta_\Gamma^{N_e} = \check{M} = \Gamma$. This requirement makes the TD-RASSCF-SP method inflexible; for an accurate description of electron correlation with keeping the numerical cost small, the orbital numbers should be $\hat{M} \geq N_e$ and $\check{M} \geq \Gamma$ as verified by the numerical

by the adjoint of both sides of Eq. (45a) gives

$$\begin{aligned} \sum_{\hat{i}\hat{j}} \langle\Psi_\gamma(t)|E_{\hat{i}}^{\hat{j}}|\Psi_\gamma(t)\rangle \mathcal{L}_{\hat{j}}^{\hat{i}}(t) \\ = \sum_{i\check{j}} \langle\Psi_{\gamma+1}(t)|E_i^{\check{j}}|\Psi_{\gamma+1}(t)\rangle \mathcal{L}_{\check{j}}^i(t), \end{aligned} \quad (46a)$$

for $\gamma = 0, \dots, \Gamma - 1$, and

$$\sum_{\hat{i}\hat{j}} \langle\Psi_\Gamma(t)|E_{\hat{i}}^{\hat{j}}|\Psi_\Gamma(t)\rangle \mathcal{L}_{\hat{j}}^{\hat{i}}(t) = 0, \quad (46b)$$

which is trivial if $\Gamma = N_e$, because of $\langle\Psi_\Gamma(t)|E_{\hat{i}}^{\hat{j}}|\Psi_\Gamma(t)\rangle = 0$. Hence the expectation value of $\mathcal{L}(t)$ [Eq. (40)] reads

demonstration in Sec. IV. Hence there appears to be an inherent defect in the Bloch operator-based formalism.

On the other hand, the formulation in Secs. II and III is designed to be free from such a problem; every TD orbital is defined excluding the bridge function $\chi_b(r)$ [see Eqs. (2a) and (2b)] and vanishes on Σ , so that two boundary conditions are from the outset imposed to each TD orbitals. This definition of the TD orbitals necessitates introducing the TI orbitals whose radial part only consists of $\chi_b(r)$. The total Hamiltonian is simply expressed by Eq. (16) without the Bloch operator as in Eq. (39), and obviously satisfies $\langle\Psi(t)|H(t)|\Psi(t)\rangle = \langle\Psi(t)|H^\dagger(t)|\Psi(t)\rangle$.

VI. CONCLUSION

As a generalization of the TD-RASSCF method [58–60] for increased numerical efficiency in the analysis of TD many-electron dynamics involving multielectron continua, the TD-RASSCF-SP method was formulated by incorporating the R -matrix-like SP concept: division of the space into a small region around the atomic nucleus (\hat{V}) and its outside (\check{V}) by a spherical surface Σ with radius r_Σ . The formulation makes use of the property of the FEDVR functions in the description of the radial motion of each electron. The wave function is expanded in terms of TD CI coefficients with Slater determinants composed of three kinds of orbitals: two sets of TD orbitals ($\hat{\mathcal{P}}$ - and $\check{\mathcal{P}}$ -space orbitals of numbers \hat{M} and \check{M} , respectively) nonvanishing only within \hat{V} and \check{V} , and a set of TI orbitals ($\check{\mathcal{P}}$ -space orbitals of numbers \check{M}) whose radial parts only consist of the bridge function across r_Σ and are hence nonvanishing only within the thin spherical shell (Σ) around Σ . Ensuring the continuous differentiability of the wave function across Σ necessitates introducing these TI orbitals. In the construction of each Slater determinant $|\Phi_{I_\gamma}(t)\rangle$, $N_e - \gamma$

orbitals are chosen from $\hat{\mathcal{P}}$, and γ are from $\check{\mathcal{P}} \oplus \bar{\mathcal{P}}$, where $\gamma = 0, \dots, \Gamma$, and $\Gamma(\leq N_e)$ denotes the maximum number of electrons in \check{V} . For comparison to understand the details of the SP strategy, another formalism is presented without introducing the TI orbitals but based upon the Bloch operator, which requires one to set $\hat{M} - \delta_\Gamma^{N_e} = \check{M} = \Gamma$ for matching the wave function on Σ . Because of this inflexibility, the Bloch operator-based formalism is not useful in practice for numerical application. On the hand, the FEDVR-based formalism allows more flexibility to set $\hat{M}(\geq N_e/2)$ and $\check{M}(\geq \Gamma/2)$.

By setting $\Gamma = 2$, for instance, the TD-RASSCF-SP theory can deal with maximally two electrons in \check{V} and hence describe dynamics involving two freed electrons after double ionization by intense lasers or electron-impact ionization of an atom. To achieve a high accuracy, the number of the $\hat{\mathcal{P}}$ -space orbitals has to be large, e.g., $\hat{M} \geq N_e$, for describing strong many-electron correlation around the nucleus, while the number of the $\check{\mathcal{P}}$ -space orbitals could be small, e.g., $\check{M} \geq \Gamma = 2$, just for capturing the weaker correlation between the two outgoing electrons in \check{V} . Hence the FEDVR-based formalism of the TD-RASSCF-SP theory will show its true potential in describing such double-continua-related phenomena. The effort to compute the TD orbitals reduces to half or less compared with that in the corresponding MCTDHF and TD-RASSCF (without SP) calculations which employ $M(\geq N_e)$ spatial orbitals in the whole volume. If the number of the TD CI coefficients is kept small, the total numerical cost is largely reduced by the SP strategy. This is the assumption on which the TD-RASSCF-SP theory is formulated. The plots of the 2D radial-electron density revealed the capability of the TD-RASSCF-SP theory to describe the double ionization induced by an intense light pulse. The numerical demonstrations, however, also revealed a practical difficulty; to fill the gap of accuracy levels between the TD and TI orbitals on Σ , the TD-RASSCF-SP calculation requires one to deploy many FEDVR functions around r_Σ . As a result, the \mathcal{Q} -space orbital

equations become stiff and necessitate setting the time step smaller ($\Delta t = 1.5 \times 10^{-4}$) than in the MCTDHF calculations ($\Delta t = 5.0 \times 10^{-4}$) for the time propagation, which means that the MCTDHF method will be faster in practice when benefitting from the larger time step. To overcome this stiffness problem requires further investigation. We believe, however, that the unique concept of the TD-RASSCF-SP theory, and the instructive discussion of its formalisms based on the FEDVR functions and the Bloch operator, will stimulate research and provoke further theoretical attempts to tackle atomic and molecular processes involving multielectron continua.

ACKNOWLEDGMENTS

This work was supported by the ERC-StG (Project No. 277767-TDMET), and the VKR center of excellence, QUSCOPE. The numerical results presented in this work were obtained at the Centre for Scientific Computing, Aarhus.

APPENDIX A: EQUATIONS OF MOTION IN THE BLOCH OPERATOR-BASED FORMALISM

For completeness and comparison to the formulation in Secs. II and III, this Appendix follows Sec. V and gives a supplementary discussion to derive the equations of motion in the Bloch operator-based formalism. The derivation goes straightforward based on the TD variational principle, and provides the formal expression of the equations of motion as in Eqs. (11) and (22). Then, substituting $H(t) = \mathcal{H}(t) - \mathcal{L}(t)$ into them leads to

$$\begin{aligned} i\dot{C}_{I,\gamma}(t) + \langle \Phi_{I,\gamma}(t) | [iD(t) - \mathcal{H}(t)] | \Psi(t) \rangle \\ + \langle \Phi_{I,\gamma}(t) | \mathcal{L}(t) | \Psi(t) \rangle = 0 \end{aligned} \quad (\text{A1})$$

and

$$\langle \Psi | E_i^a (iD - \mathcal{H}(t)) | \Psi \rangle + \langle \Psi | E_i^a \mathcal{L}(t) | \Psi \rangle = 0. \quad (\text{A2})$$

More explicit forms of these equations are derived below.

1. Encompassing the matching condition

To proceed, letting $\mathcal{L}(t)$ operate on $|\Psi_\gamma(t)\rangle$ as follows is useful to encompass the matching condition:

$$\begin{aligned} \mathcal{L}(t)|\Psi_\gamma(t)\rangle &= \sum_{\hat{p}\hat{j}} E_{\hat{p}}^{\hat{j}} |\Psi_\gamma(t)\rangle \mathcal{L}_{\hat{j}}^{\hat{p}}(t) - \sum_{\check{p}\check{j}} E_{\check{p}}^{\check{j}} |\Psi_\gamma(t)\rangle \mathcal{L}_{\check{j}}^{\check{p}}(t) \\ &= \sum_{\hat{p}\check{j}} E_{\hat{p}}^{\check{j}} |\Psi_{\gamma+1}(t)\rangle \mathcal{L}_{\check{j}}^{\hat{p}}(t) + \delta_\gamma^\Gamma \sum_{\hat{p}\hat{j}} E_{\hat{p}}^{\hat{j}} |\Psi_\Gamma(t)\rangle \mathcal{L}_{\hat{j}}^{\hat{p}}(t) - \sum_{\check{p}\hat{j}} E_{\check{p}}^{\hat{j}} |\Psi_{\gamma-1}(t)\rangle \mathcal{L}_{\hat{j}}^{\check{p}}(t), \end{aligned} \quad (\text{A3})$$

where $\gamma = 0, \dots, \Gamma$, with $|\Psi_{-1}(t)\rangle \equiv |\Psi_{\Gamma+1}(t)\rangle \equiv 0$. The definition of $\mathcal{L}(t)$ [Eq. (40)] immediately gives the first line, which leads to the second line with using Eq. (45b) and defining

$$\mathcal{L}_{\check{q}}^{\check{p}}(t) = \frac{1}{2} \int d\Omega \left[\phi_{\check{p}}^*(\mathbf{r}, t)|_{r=r_\Sigma+0} \frac{\partial}{\partial r} \phi_{\check{q}}(\mathbf{r}, t)|_{r=r_\Sigma} \right], \quad (\text{A4a})$$

$$\mathcal{L}_{\hat{q}}^{\hat{p}}(t) = \frac{1}{2} \int d\Omega \left[\phi_{\hat{p}}^*(\mathbf{r}, t)|_{r=r_\Sigma} \frac{\partial}{\partial r} \phi_{\hat{q}}(\mathbf{r}, t)|_{r=r_\Sigma+0} \right]. \quad (\text{A4b})$$

Taking summation on both sides of Eq. (A3) over $\gamma = 0, \dots, \Gamma$ then leads to

$$\mathcal{L}(t)|\Psi(t)\rangle = \sum_{\check{p}\check{j}} E_{\check{p}}^{\check{j}} |\Psi(t)\rangle \mathcal{L}_{\check{j}}^{\check{p}}(t) + \sum_{\hat{p}\hat{j}} E_{\hat{p}}^{\hat{j}} |\Psi_\Gamma(t)\rangle \mathcal{L}_{\hat{j}}^{\hat{p}}(t) \sum_{\check{p}\hat{j}} E_{\check{p}}^{\hat{j}} |\Psi(t)\rangle \mathcal{L}_{\hat{j}}^{\check{p}}(t), \quad (\text{A5})$$

where the second term on the right-hand side disappears for $\Gamma = N_e$ because $|\Psi_{\Gamma(N_e)}(t)\rangle$ contains no electron in \hat{V} .

2. Explicit expression of the equations of motion

a. Amplitude equations

Using Eq. (A5) in Eq. (A1) and collecting only nonvanishing terms gives

$$\begin{aligned} i\dot{C}_{I_\gamma}(t) = & \sum_{\hat{i}\hat{j}} h_{\hat{j}}^{\hat{i}}(t)\langle\Phi_{I_\gamma}(t)|E_{\hat{i}}^{\hat{j}}|\Psi_\gamma(t)\rangle + \sum_{\check{i}\check{j}} h_{\check{j}}^{\check{i}}(t)\langle\Phi_{I_\gamma}(t)|E_{\check{i}}^{\check{j}}|\Psi_\gamma(t)\rangle \\ & + \frac{1}{2} \sum_{\hat{i}\hat{j}\hat{k}\hat{l}} v_{\hat{j}\hat{l}}^{\hat{i}\hat{k}}(t)\langle\Phi_{I_\gamma}(t)|E_{\hat{i}\hat{k}}^{\hat{j}\hat{l}}|\Psi_\gamma(t)\rangle + \frac{1}{2} \sum_{\check{i}\check{j}\check{k}\check{l}} v_{\check{j}\check{l}}^{\check{i}\check{k}}(t)\langle\Phi_{I_\gamma}(t)|E_{\check{i}\check{k}}^{\check{j}\check{l}}|\Psi_\gamma(t)\rangle + \sum_{\hat{i}\hat{j}\hat{k}\hat{l}} v_{\hat{j}\hat{l}}^{\hat{i}\hat{k}}(t)\langle\Phi_{I_\gamma}(t)|E_{\hat{i}\hat{k}}^{\hat{j}\hat{l}}|\Psi_\gamma(t)\rangle \\ & - \sum_{\check{i}\check{j}} \mathcal{L}_{\check{j}}^{\check{i}}(t)\langle\Phi_{I_\gamma}(t)|E_{\check{i}}^{\check{j}}|\Psi_{\gamma+1}(t)\rangle - \delta_\gamma^\Gamma \sum_{\hat{i}\hat{j}} \mathcal{L}_{\hat{j}}^{\hat{i}}(t)\langle\Phi_{I_\Gamma}(t)|E_{\hat{i}}^{\hat{j}}|\Psi_\Gamma(t)\rangle + \sum_{\check{i}\check{j}} \mathcal{L}_{\check{j}}^{\check{i}}(t)\langle\Phi_{I_\gamma}(t)|E_{\check{i}}^{\check{j}}|\Psi_{\gamma-1}(t)\rangle, \end{aligned} \quad (\text{A6})$$

where $\gamma = 0, \dots, \Gamma$. Compare with Eq. (21) and notice the relation between \mathcal{L} and u . Now the Bloch operator takes the role of coupling electronic states of different values of γ .

b. \mathcal{Q} -space orbital equations

The detailed consideration of the first term on the left-hand side of Eq. (A2) formally follows the same procedure as from Eqs. (22) to (24) in Sec. III B 2. On the other hand, the second term, using Eq. (A5), leads to

$$\begin{aligned} \langle\Psi(t)|E_{\hat{i}}^{\hat{a}}\mathcal{L}(t)|\Psi(t)\rangle &= \sum_{\gamma=0}^{\Gamma-1} \sum_{\check{j}} \mathcal{L}_{\check{j}}^{\hat{a}}(t)\langle\Psi_\gamma(t)|E_{\check{i}}^{\check{j}}|\Psi_{\gamma+1}(t)\rangle + \sum_{\hat{j}} \mathcal{L}_{\hat{j}}^{\hat{a}}(t)\langle\Psi_\Gamma(t)|E_{\hat{i}}^{\hat{j}}|\Psi_\Gamma(t)\rangle \\ &\equiv \sum_{\check{j}} \mathcal{L}_{\check{j}}^{\hat{a}}(t)\rho_{\check{i}}^{\check{j}}(t) + \sum_{\hat{j}} \mathcal{L}_{\hat{j}}^{\hat{a}}(t)\langle\Psi_\Gamma(t)|E_{\hat{i}}^{\hat{j}}|\Psi_\Gamma(t)\rangle, \end{aligned} \quad (\text{A7a})$$

for the pair of orbital indices (\hat{i}, \hat{a}) , and

$$\langle\Psi(t)|E_{\check{i}}^{\check{a}}\mathcal{L}(t)|\Psi(t)\rangle = - \sum_{\gamma=1}^{\Gamma} \sum_{\hat{j}} \mathcal{L}_{\hat{j}}^{\check{a}}(t)\langle\Psi_\gamma(t)|E_{\check{i}}^{\check{j}}|\Psi_{\gamma-1}(t)\rangle \equiv - \sum_{\hat{j}} \mathcal{L}_{\hat{j}}^{\check{a}}(t)\rho_{\check{i}}^{\check{j}}(t), \quad (\text{A7b})$$

for the other pair (\check{i}, \check{a}) , where $\rho_{\check{i}}^{\check{j}}(t)$ and $\rho_{\check{i}}^{\check{j}}(t)$ are, respectively, defined by the second equivalences in Eqs. (A7a) and (A7b). Hence Eq. (A2) is recast into forms as follows:

$$\sum_{\hat{j}} [i\eta_{\hat{j}}^{\hat{a}}(t) - h_{\hat{j}}^{\hat{a}}(t)]\rho_{\hat{i}}^{\hat{j}}(t) - \sum_{\hat{j}\hat{k}\hat{l}} v_{\hat{j}\hat{l}}^{\hat{a}\hat{k}}(t)\rho_{\hat{i}\hat{k}}^{\hat{j}\hat{l}}(t) + \sum_{\check{j}} \mathcal{L}_{\check{j}}^{\hat{a}}(t)\rho_{\check{i}}^{\check{j}}(t) + \sum_{\hat{j}} \mathcal{L}_{\hat{j}}^{\hat{a}}(t)\langle\Psi_\Gamma(t)|E_{\hat{i}}^{\hat{j}}|\Psi_\Gamma(t)\rangle = 0, \quad (\text{A8a})$$

$$\sum_{\check{j}} [i\eta_{\check{j}}^{\check{a}}(t) - h_{\check{j}}^{\check{a}}(t)]\rho_{\check{i}}^{\check{j}}(t) - \sum_{\check{j}\check{k}\check{l}} v_{\check{j}\check{l}}^{\check{a}\check{k}}(t)\rho_{\check{i}\check{k}}^{\check{j}\check{l}}(t) - \sum_{\hat{j}} \mathcal{L}_{\hat{j}}^{\check{a}}(t)\rho_{\check{i}}^{\check{j}}(t) = 0. \quad (\text{A8b})$$

Then following the same manipulation as in Sec. III B 2, the \mathcal{Q} -space orbital equations in the inner and outer regions, respectively, are given by

$$i \sum_{\hat{j}} \hat{Q}(t)|\dot{\phi}_{\hat{j}}(t)\rangle\rho_{\hat{i}}^{\hat{j}}(t) = \hat{Q}(t) \left\{ \sum_{\hat{j}} \left[\rho_{\hat{i}}^{\hat{j}}(t)h(t) + \sum_{kl} \rho_{ik}^{\hat{j}l}W_l^k(t) - \langle\Psi_\Gamma(t)|E_{\hat{i}}^{\hat{j}}|\Psi_\Gamma(t)\rangle\mathcal{L} \right] |\phi_{\hat{j}}(t)\rangle - \sum_{\check{j}} \mathcal{L}|\phi_{\check{j}}(t)\rangle\rho_{\check{i}}^{\check{j}}(t) \right\}, \quad (\text{A9a})$$

$$i \sum_{\check{j}} \check{Q}(t)|\dot{\phi}_{\check{j}}(t)\rangle\rho_{\check{i}}^{\check{j}}(t) = \check{Q}(t) \left\{ \sum_{\check{j}} \left[\rho_{\check{i}}^{\check{j}}(t)h(t) + \sum_{kl} \rho_{ik}^{\check{j}l}W_l^k(t) \right] |\phi_{\check{j}}(t)\rangle + \sum_{\hat{j}} \mathcal{L}|\phi_{\hat{j}}(t)\rangle\rho_{\hat{i}}^{\hat{j}}(t) \right\}. \quad (\text{A9b})$$

Compare with Eq. (26), and notice the relation between \mathcal{L} and u . The Bloch operator accounts for the boundary conditions on Σ .

APPENDIX B: SUMMARY OF NOTATION RULES

The notation rules introduced in Sec.1 II C are summarized below.

1. Single-particle Hilbert spaces:

$$\mathcal{P} = \begin{cases} \hat{\mathcal{P}} \equiv \{\phi_i(\mathbf{r}, t)\}_{i=1}^{\hat{M}}, \\ \check{\mathcal{P}} \equiv \{\phi_i(\mathbf{r}, t)\}_{i=\hat{M}+1}^{\hat{M}+\check{M}}, \\ \bar{\mathcal{P}} \equiv \{\phi_{\bar{i}}(\mathbf{r})\}_{\bar{i}=\hat{M}+\check{M}+1}^{\hat{M}+\check{M}+\bar{M}} \end{cases} \quad (\text{B1a})$$

and

$$\mathcal{Q} = \begin{cases} \hat{\mathcal{Q}} \equiv \{\phi_{\hat{a}}(\mathbf{r}, t)\}_{\hat{a}}, \\ \check{\mathcal{Q}} \equiv \{\phi_{\check{a}}(\mathbf{r}, t)\}_{\check{a}}. \end{cases} \quad (\text{B1b})$$

2. Orbitals:

$$\phi_p(\mathbf{r}, t) = \begin{cases} \phi_{\hat{p}}(\mathbf{r}, t) = \begin{cases} \phi_i(\mathbf{r}, t), \\ \phi_{\hat{a}}(\mathbf{r}, t), \end{cases} \\ \phi_{\check{p}}(\mathbf{r}, t) = \begin{cases} \phi_i(\mathbf{r}, t), \\ \phi_{\check{a}}(\mathbf{r}, t), \end{cases} \\ \phi_{\bar{i}}(\mathbf{r}), \end{cases} \quad (\text{B2a})$$

$$\phi_i(\mathbf{r}, t) = \begin{cases} \phi_i(\mathbf{r}, t), \\ \phi_{\hat{i}}(\mathbf{r}, t), \\ \phi_{\check{i}}(\mathbf{r}), \end{cases} \quad (\text{B2b})$$

and

$$\phi_a(\mathbf{r}, t) = \begin{cases} \phi_{\hat{a}}(\mathbf{r}, t), \\ \phi_{\check{a}}(\mathbf{r}, t). \end{cases} \quad (\text{B2c})$$

Notice that $\phi_p(\mathbf{r}, t)$ and $\phi_i(\mathbf{r}, t)$ seem time dependent, but could denote $\phi_{\bar{i}}(\mathbf{r})$ and hence be time independent.

3. FEDVR functions:

$$\chi_k(r) = \begin{cases} \chi_{\hat{k}}(r), \\ \chi_{\check{k}}(r), \\ \chi_b(r) = [\hat{\chi}_b(r) + \check{\chi}_b(r)]/\sqrt{2}. \end{cases} \quad (\text{B3})$$

-
- [1] P. M. Paul, E. S. Toma, P. Breger, G. Mullot, F. Augé, Ph. Balcoun, H. G. Muller, and P. Agostini, Observation of a train of attosecond pulses from high harmonic generation, *Science* **291**, 1689 (2001).
- [2] R. Kienberger, E. Goulielmakis, M. Uiberacker, A. Baltuska, V. Yakovlev, F. Bammer, A. Scrinzi, Th. Westerwalbesloh, U. Kleineberg, U. Heinzmann, M. Drescher, and F. Krausz, Atomic transient recorder, *Nature (London)* **427**, 817 (2004).
- [3] T. Popmintchev, M.-C. Chen, P. Arpin, M. M. Murnane, and H. C. Kapteyn, The attosecond nonlinear optics of bright coherent x-ray generation, *Nat. Photon.* **4**, 822 (2010).
- [4] P. Bucksbaum, T. Möller, and K. Ueda, Frontiers of free-electron laser science, *J. Phys. B* **46**, 160201 (2013).
- [5] R. Falcone, M. Dunne, H. Chapman, M. Yabashi, and K. Ueda, Frontiers of free-electron laser science II, *J. Phys. B* **49**, 180201 (2016).
- [6] L. A. A. Nikolopoulos, Time-Dependent Theory of Angular Correlations in Sequential Double Ionization, *Phys. Rev. Lett.* **111**, 093001 (2013).
- [7] E. P. Måansson, D. Guénot, C. L. Arnold, D. Kroon, S. Kasper, J. M. Dahlström, E. Lindroth, A. S. Kheifets, A. L'Huillier, S. L. Sorensen, and M. Gisselbrecht, Double ionization probed on the attosecond timescale, *Nat. Phys.* **10**, 207 (2014).
- [8] K. C. Kulander, K. J. Schafer, and J. L. Krause, in *Atoms in Intense Radiation Fields*, edited by M. Gavrila (Academic Press, New York, 1992), pp. 247–300.
- [9] E. P. Wigner, Resonance reactions and anomalous scattering, *Phys. Rev.* **70**, 15 (1946).
- [10] E. P. Wigner, Resonance reactions, *Phys. Rev.* **70**, 606 (1946).
- [11] E. P. Wigner and L. Eisenbud, Higher angular momenta and long range interaction in resonance reactions, *Phys. Rev.* **72**, 29 (1947).
- [12] P. Descouvemont and D. Baye, The *R*-matrix theory, *Rep. Prog. Phys.* **73**, 036301 (2010).
- [13] P. G. Burke, *R-Matrix Theory of Atomic Collisions* (Springer-Verlag, Heidelberg, 2011).
- [14] P. G. Burke and V. M. Burke, Time-dependent *R*-matrix theory of multiphoton processes, *J. Phys. B* **30**, L383 (1997).
- [15] M. A. Lysaght, H. W. van der Hart, and P. G. Burke, Time-dependent *R*-matrix theory for ultrafast atomic processes, *Phys. Rev. A* **79**, 053411 (2009).
- [16] A. C. Brown, D. J. Robinson, and H. W. van der Hart, Atomic harmonic generation in time-dependent *R*-matrix theory, *Phys. Rev. A* **86**, 053420 (2012).
- [17] M. A. Lysaght, P. G. Burke, and H. W. van der Hart, Ultrafast Probing of Collective Electron Dynamics Driven by Dielectronic Repulsion, *Phys. Rev. Lett.* **102**, 193001 (2009).

- [18] M. A. Lysaght, S. Hutchinson, and H. W. van der Hart, Signatures of collective electron dynamics in the angular distributions of electrons ejected during ultrashort laser pulse interactions with C⁺, *New J. Phys.* **11**, 093014 (2009).
- [19] M. A. Lysaght, P. G. Burke, and H. W. van der Hart, Ultrafast Laser-Driven Excitation Dynamics in Ne: An *Ab Initio* Time-Dependent *R*-Matrix Approach, *Phys. Rev. Lett.* **101**, 253001 (2008).
- [20] O. Hassouneh, A. C. Brown, and H. W. van der Hart, Multichannel interference in high-order-harmonic generation from Ne⁺ driven by an ultrashort intense laser pulse, *Phys. Rev. A* **89**, 033409 (2014).
- [21] A. C. Brown, S. Hutchinson, M. A. Lysaght, and H. W. van der Hart, Interference Between Competing Pathways in Atomic Harmonic Generation, *Phys. Rev. Lett.* **108**, 063006 (2012).
- [22] S. Hutchinson, M. A. Lysaght, and H. W. van der Hart, Anisotropy parameters in two-color two-photon above-threshold ionization, *Phys. Rev. A* **88**, 023424 (2013).
- [23] A. C. Brown and H. W. van der Hart, Influence of multiple ionization thresholds on harmonic generation from Ar⁺, *Phys. Rev. A* **86**, 063416 (2012).
- [24] A. C. Brown and H. W. van der Hart, Enhanced harmonic generation from Ar⁺ aligned with $M = 1$, *Phys. Rev. A* **88**, 033419 (2013).
- [25] L. A. A. Nikolopoulos, J. S. Parker, and K. T. Taylor, Combined *R*-matrix eigenstate basis set and finite-difference propagation method for the time-dependent Schrödinger equation: The one-electron case, *Phys. Rev. A* **78**, 063420 (2008).
- [26] L. R. Moore, M. A. Lysaght, L. A. A. Nikolopoulos, J. S. Parker, H. W. van der Hart, and K. T. Taylor, The RMT method for many-electron atomic systems in intense short-pulse laser light, *J. Mod. Opt.* **58**, 1132 (2011).
- [27] H. W. van der Hart, Time-dependent *R*-matrix theory applied to two-photon double ionization of He, *Phys. Rev. A* **89**, 053407 (2014).
- [28] C. O'Broin and L. A. A. Nikolopoulos, *R*-matrix-incorporating-time method for H₂⁺ in short and intense laser fields, *Phys. Rev. A* **92**, 063428 (2015).
- [29] C. Bloch, Une formulation unifiée de la théorie des réactions nucléaires, *Nucl. Phys.* **4**, 503 (1957).
- [30] W. E. Arnoldi, The principle of minimized iterations in the solution of the matrix eigenvalue problem, *Quart. Appl. Math.* **9**, 17 (1951).
- [31] T. J. Park and J. C. Light, Unitary quantum time evolution by iterative Lanczos reduction, *J. Chem. Phys.* **85**, 5870 (1986).
- [32] L. R. Moore, M. A. Lysaght, J. S. Parker, H. W. van der Hart, and K. T. Taylor, Time delay between photoemission from the 2p and 2s subshells of neon, *Phys. Rev. A* **84**, 061404(R) (2011).
- [33] H. W. van der Hart and R. Morgan, Population trapping in bound states during IR-assisted ultrafast photoionization of Ne⁺, *Phys. Rev. A* **90**, 013424 (2014).
- [34] H. F. Rey and H. W. van der Hart, Probing spin-orbit-interaction-induced electron dynamics in the carbon atom by multiphoton ionization, *Phys. Rev. A* **90**, 033402 (2014).
- [35] O. Hassouneh, A. C. Brown, and H. W. van der Hart, Harmonic generation by noble-gas atoms in the near-IR regime using *ab initio* time-dependent *R*-matrix theory, *Phys. Rev. A* **90**, 043418 (2014).
- [36] O. Hassouneh, S. Law, S. F. C. Shearer, A. C. Brown, and H. W. van der Hart, Electron rescattering in strong-field photodetachment of F⁻, *Phys. Rev. A* **91**, 031404(R) (2015).
- [37] H. F. Rey and H. W. van der Hart, Multiphoton inner-shell ionization of the carbon atom, *Phys. Rev. A* **92**, 013417 (2015).
- [38] A. C. Brown and H. W. van der Hart, Extreme-Ultraviolet-Initiated High-Order Harmonic Generation: Driving Inner-Valance Electrons Using Below-Threshold-Energy Extreme-Ultraviolet Light, *Phys. Rev. Lett.* **117**, 093201 (2016).
- [39] D. Hochstuhl and M. Bonitz, Time-dependent restricted-active-space configuration-interaction method for the photoionization of many-electron atoms, *Phys. Rev. A* **86**, 053424 (2012).
- [40] D. Hochstuhl, C. M. Hinz, and M. Bonitz, Time-dependent multiconfiguration methods for the numerical simulation of photoionization processes of many-electron atoms, *Eur. Phys. J. Spec. Top.* **223**, 117 (2014).
- [41] S. Bauch, L. K. Sørensen, and L. B. Madsen, Time-dependent generalized-active-space configuration-interaction approach to photoionization dynamics of atoms and molecules, *Phys. Rev. A* **90**, 062508 (2014).
- [42] T. N. Rescigno and C. W. McCurdy, Numerical grid methods for quantum-mechanical scattering problems, *Phys. Rev. A* **62**, 032706 (2000).
- [43] L. Torlina and O. Smirnova, Time-dependent analytical *R*-matrix approach for strong-field dynamics. I. One-electron systems, *Phys. Rev. A* **86**, 043408 (2012).
- [44] L. Torlina, M. Ivanov, Z. B. Walters, and O. Smirnova, Time-dependent analytical *R*-matrix approach for strong-field dynamics. II. Many-electron systems, *Phys. Rev. A* **86**, 043409 (2012).
- [45] J. Kaushal and O. Smirnova, Nonadiabatic Coulomb effects in strong-field ionization in circularly polarized laser fields, *Phys. Rev. A* **88**, 013421 (2013).
- [46] L. Torlina, J. Kaushal, and O. Smirnova, Time-resolving electron-core dynamics during strong-field ionization in circularly polarized fields, *Phys. Rev. A* **88**, 053403 (2013).
- [47] L. Torlina, F. Morales, J. Kaushal, I. Ivanov, A. Kheifets, A. Zielinski, A. Scrinzi, H. G. Muller, S. Sukiasyan, M. Ivanov, and O. Smirnova, Interpreting attoclock measurements of tunneling times, *Nat. Phys.* **11**, 503 (2015).
- [48] J. Wragg, J. S. Parker, and H. W. van der Hart, Double ionization in *R*-matrix theory using a two-electron outer region, *Phys. Rev. A* **92**, 022504 (2015).
- [49] J. Wragg and H. W. van der Hart, Spin and spatial dynamics in electron-impact scattering of S-wave He using *R*-matrix with time-dependence theory, *Phys. Rev. A* **94**, 032706 (2016).
- [50] H. D. Meyer, U. Manthe, and L. S. Cederbaum, The multi-configurational time-dependent Hartree approach, *Chem. Phys. Lett.* **165**, 73 (1990).
- [51] M. H. Beck, A. Jäckle, G. A. Worth, and H. D. Meyer, The multiconfiguration time-dependent Hartree (MCTDH) method: a highly efficient algorithm for propagating wavepackets, *Phys. Rep.* **324**, 1 (2000).
- [52] J. Caillat, J. Zanghellini, M. Kitzler, O. Koch, W. Kreuzer, and A. Scrinzi, Correlated multielectron systems in strong laser fields: A multiconfiguration time-dependent Hartree-Fock approach, *Phys. Rev. A* **71**, 012712 (2005).

- [53] H. D. Meyer, F. Gatti, and G. A. Worth, *Multidimensional Quantum Dynamics* (Wiley-VCH, Weinheim, 2010).
- [54] M. Nest, R. Padmanaban, and P. Saalfrank, Time-dependent approach to electronically excited states of molecules with the multiconfiguration time-dependent Hartree-Fock method, *J. Chem. Phys.* **126**, 214106 (2007).
- [55] D. J. Haxton, K. V. Lawler, and C. W. McCurdy, Multiconfiguration time-dependent Hartree-Fock treatment of electronic and nuclear dynamics in diatomic molecules, *Phys. Rev. A* **83**, 063416 (2011).
- [56] D. J. Haxton, K. V. Lawler, and C. W. McCurdy, Single photoionization of Be and HF using the multiconfiguration time-dependent Hartree-Fock method, *Phys. Rev. A* **86**, 013406 (2012).
- [57] D. Hochstuhl and M. Bonitz, Two-photon ionization of helium studied with the multiconfigurational time-dependent Hartree-Fock method, *J. Phys. Chem.* **134**, 084106 (2011).
- [58] H. Miyagi and L. B. Madsen, Time-dependent restricted-active-space self-consistent-field theory for laser-driven many-electron dynamics, *Phys. Rev. A* **87**, 062511 (2013).
- [59] H. Miyagi and L. B. Madsen, Time-dependent restricted-active-space self-consistent-field singles method for many-electron dynamics, *J. Chem. Phys.* **140**, 164309 (2014).
- [60] H. Miyagi and L. B. Madsen, Time-dependent restricted-active-space self-consistent-field theory for laser-driven many-electron dynamics. II. Extended formulation and numerical analysis, *Phys. Rev. A* **89**, 063416 (2014).
- [61] T. Sato and K. L. Ishikawa, Time-dependent complete-active-space self-consistent-field method for multielectron dynamics in intense laser fields, *Phys. Rev. A* **88**, 023402 (2013).
- [62] T. Sato and K. L. Ishikawa, Time-dependent multiconfiguration self-consistent-field method based on the occupation-restricted multiple-active-space model for multielectron dynamics in intense laser fields, *Phys. Rev. A* **91**, 023417 (2015).
- [63] T. Sato, K. L. Ishikawa, I. Březinová, F. Lackner, S. Nagele, and J. Burgdörfer, Time-dependent complete-active-space self-consistent-field method for atoms: Application to high-order harmonic generation, *Phys. Rev. A* **94**, 023405 (2016).
- [64] D. J. Haxton and C. W. McCurdy, Two methods for restricted configuration spaces within the multiconfiguration time-dependent Hartree-Fock method, *Phys. Rev. A* **91**, 012509 (2015).
- [65] A. S. Simonsen, H. Bachau, and M. Førre, Two-photon double ionization of metastable ${}^{1,3}S\ 1s2s$ helium, *Phys. Rev. A* **89**, 043427 (2014).
- [66] Th. Weber, H. Giessen, M. Weckenbrock, G. Urbasch, A. Staudte, L. Spielberger, O. Jagutzki, V. Mergel, M. Vollmer, and R. Dörner, Correlated electron emission in multiphoton double ionization, *Nature (London)* **405**, 658 (2000).
- [67] H. Miyagi and L. B. Madsen, Exterior time scaling with the stiffness-free Lanczos time propagator: Formulation and application to atoms interacting with strong midinfrared lasers, *Phys. Rev. A* **93**, 033420 (2016).
- [68] P. Kramer and M. Saraceno, *Geometry of the Time-dependent Variational Principle in Quantum Mechanics*, Lecture Notes in Physics Vol. 140 (Springer-Verlag, Berlin, 1981).
- [69] C. Lubich, *From Quantum to Classical Molecular Dynamics: Reduced Models and Numerical Analysis* (European Mathematical Society, Zürich, 2008).
- [70] T. Helgaker, P. Jørgensen, and J. Olsen, *Molecular Electronic Structure Theory* (Wiley, New York, 2000).
- [71] I. Shavitt and R. J. Bartlett, *Many-Body Methods in Chemistry and Physics—MBPT and Coupled-Cluster Theory* (Cambridge University Press, Cambridge, UK, 2009).
- [72] R. Kosloff and H. Tal-Ezer, A direct relaxation method for calculating eigenfunctions and eigenvalues of the Schrödinger equation on a grid, *Chem. Phys. Lett.* **127**, 223 (1986).
- [73] J. Zanghellini, Ch. Jungreuthmayer, and T. Brabec, Plasmon signatures in high harmonic generation, *J. Phys. B* **39**, 709 (2006).
- [74] E. Merzbacher, *Quantum Mechanics*, 3rd ed. (John Wiley & Sons, New York, 1998).